A FOCUSING X-RAY TELESCOPE FOR HIGH ALTITUDE OBSERVATIONS OF COSMIC X-RAYS IN THE ENERGY RANGE 20-140 KeV

by

THOMAS RUSSELL LINDQUIST

School of Physics and Astronomy
University of Minnesota
Minneapolis, Minnesota

Technical Report CR-110

DECEMBER, 1967

In partial fulfillment of the requirements for the Degree of Master of Science.

ACKNOWLEDGMENTS

I wish to thank my advisor, Dr. William R. Webber, for his support of this project.

I am also grateful to Steven Blake, Jeffrey Hammer, Marie Gibson, Laura Danske, Gilbert Ahlstrand, John Dvoracek, and Mary Potasek for their help in building some very useful mechanical and optical devices, cleaving four thousand salt crystals, assisting in many measurements of x-ray reflecting power, and helping assemble the x-ray lens.

Thanks are also due to John Rockstroh and Michael Dougherty for writing the computer program from my basic outline.

Finally I wish to thank Mr. Jack Brumbaugh, Mr. Carson B. Trenor, and others of the Morton Salt Company for providing us with the crude rock salt for this project.

TABLE OF CONTENTS

I. THE STATE OF X-RAY ASTRONOMY

In June of 1962, a rocket payload carrying x-ray detectors was launched in an attempt to see if the moon emitted x-rays (a possible consequence of impinging solar x-rays). No lunar x-rays were detected, but a powerful source of x-rays in the constellation Scorpius was discovered (Bowyer et al., 1964). Thus x-ray astronomy was born.

Since then, nearly forty discreet sources of cosmic x-rays have been located by rocket-borne detectors (Friedman, 1967). Only the strongest of these sources have been observed by balloon-borne detectors. There also exists an apparently isotropic background of extraterrestrial x-rays, detected by balloon experiments (Brini et al., 1967) as well as rocket payloads (Friedman, 1967). The most intense sources are Sco X-1 (identified with an old nova of optical magnitude $\tilde{=}$ 8), Crux X-1 (not yet identified with any optical object (McCracken, 1967)), Cyg X-1 (also unidentified optically), Cyg X-2 (tentatively identified with an object of visual magnitude $\tilde{=}$ 15.5 (Giacconi et al., 1967)), and Tau X-1 (the Crab Nebula, a supernova remnant). The optical identifications of Sco X-1 and Cyg X-2 were made by narrowing the search to optical objects whose visual magnitude and colors (B-V and U-B) were consistent with a flat emission spectrum (energy per unit frequency interval) from x-ray to visible frequencies, an assumption which is valid if the photons throughout this range are produced by bremsstrahlung in an optically thin plasma or

by synchrotron radiation from free electrons with a flat energy distribution (Giacconi et al., 1967). The most recently discovered x-ray emitters include the radio galaxy M87 and the quasi-stellar object 3C237 (Friedman, 1967), the first extra-galactic objects so identified.

Rocket-borne detectors typically consist of geiger or proportional counters which are efficient at wavelengths between 1.5 and 8 Angstrom units (energies between 8.3 and 1.55 KeV). Balloon-borne detectors, however, are severely limited by atmospheric absorption at energies below about 20 KeV. The experiments flown thus far on balloons have used sodium iodide scintillation crystals and photomultiplier tubes, usually in conjunction with passive and active shielding to narrow the detector's field of view. The most effective active shield is a scintillating crystal such as cesium iodide, which has a large absorption coefficient for x-rays and gamma rays. This "guard" scintillator is operated in anticoincidence with the central detector; that is, pulses from the central detector are analyzed only if there is not a simultaneous pulse from the guard scintillator's photomultiplier tube.

But even with cesium iodide or sodium iodide guard scintillators a few centimeters thick, a large amount of background radiation still reaches the central detector. With detectors of this type, Peterson et al. (1965) and Haymes and Craddock (1966) obtained x-ray counting rates from the Crab Nebula only about 70% as great as their detectors' background counting rates, in

the energy range 20-50 KeV. At other energies, the signal to background ratio is considerably worse.

This background might largely be due to high energy x-rays and gamma rays (produced in the upper atmosphere by cosmic rays) which can pass undetected through the guard and lose a fraction of their original energy by the Compton effect in the central detector. They are thus experimentally indistinguishable from low energy x-rays which come through the experiment's forward aperture and lose all their energy in the central detector by the photoelectric effect (the dominant energy-loss process at energies below about 200 KeV).

II. ATTEMPTS TO IMPROVE BALLOON-BORNE DETECTORS

The sensitivity of a balloon experiment can be improved by increasing the detector's area or exposure time. (The total number N of events due to a source will be proportional to the area time product, AT, while a standard deviation σ in the number of background events will be proportional to $\sqrt{AT}$; thus $N/\sigma \propto \sqrt{AT}$.) Increasing the central detector area to more than about 50 square centimeters requires expensive anticoincidence scintillators (more than $10,000.00 if cesium iodide is used). A fundamental limitation on exposure time is imposed by the earth's rotation (15° per hour) and the strong absorption of x-rays at zenith angles much greater than 30°. To even utilize fully this four hour interval, a pointing control system capable of tracking the source across the sky must be used.

As an alternate approach to the problem of increasing the sensitivity of a balloon-borne x-ray detector, I have considered various ways of focusing "hard" (of wavelength shorter than an Angstrom unit) x-rays from a large collection area to a small focal area (where a conventional sodium iodide crystal would be located). To efficiently reflect x-rays of wavelength $\lambda \lesssim 1$Å (energy $E \gtrsim 12.4$ KeV), one must use Bragg reflection from a crystal with interplanar distances no greater than a few Angstrom units. Figure 1 shows three possible arrangements in which crystals at points P and P' cause reflected x-rays to converge to a focal point O. Reflection from a given crystal can only occur if the

Bragg condition

$$n\lambda = 2d \sin\theta \qquad (1)$$

is satisfied or very nearly satisfied. (Here n is the order of the reflection, d is the distance between the reflecting planes of the crystal, and θ is the glancing angle.) Since θ depends on the coordinates of P, different crystals reflect effectively at different energies.

Most crystals have interplanar distances greater than 2 or 3 Angstrom units. This, along with a desired low energy limit of about 15 KeV, necessitates glancing angles $\theta \lesssim 10°$ for first order (by far the strongest) reflections. Thus the geometry of Figure 1 (a) (in which $\theta > 45°$ for all reflecting crystals) is ruled out.

The geometries of Figure 1 (b) and (c) are further compared in Figure 2, which illustrates the difference between the Bragg and Laue cases of reflection. In the Bragg case (Figure 2 (a)) the reflected beam leaves the face it entered whereas in the Laue case (Figure 2 (b)) the reflected beam leaves a different face, parallel to that which it entered. For near-optimum efficiency in the Bragg case, the maximum path length in the crystal, $\frac{2T_B}{\sin\theta}$ must be more than one absorption length, Λ. (An absorption length is the distance traveled by the incident beam in the crystal before its intensity is reduced by a factor of e.) Thus the crystal thickness in the Bragg case should satisfy

$$T_B \gtrsim \Lambda \frac{\sin\theta}{2} . \qquad (2)$$

Using a crystal much thicker than this will slightly increase the intensity reflected from this particular crystal, but will prevent the closest possible spacing of adjacent crystals and thus will waste space. The optimum crystal thickness for the Bragg case is thus about $\Lambda \frac{\sin \theta}{2}$.

Similarly, in the Laue case the efficiency of reflection is greatest if the path length, $\frac{T_L}{\cos \theta}$, is about one absorption length. (The probability of reflection increases linearly with thickness until absorption becomes significant.) Thus

$$T_L \tilde{=} \Lambda \cos \theta. \qquad (3)$$

In both cases, the individual crystal's horizontal dimension "w" (see Figure 2) must be less than the diameter of the detector (which is centered at the focal point) so that all reflected x-rays will be detected.

Thus, for small θ, the crystals used in the Bragg case should be much thinner ($\frac{T_B}{T_L} \tilde{=} \frac{\sin \theta}{2 \cos \theta}$) than those used in the Laue case. And if a single crystal is used to intercept x-rays over a distance w, that crystal must have length $\ell = \frac{w}{\sin \theta}$ in the Bragg case, but only $\frac{w}{\cos \theta}$ in the Laue case. The more convenient crystal dimensions used in the Laue case make the geometry of Figure 1 (c) the best for our application.

III. THE X-RAY "LENS"

The x-ray telescope was accordingly designed as shown schematically in Figure 3 (which is not a scale drawing). Its "lens" consists of approximately 4000 rock salt crystals (cleaved from large, natural chunks from a Morton Salt Company mine at Grand Saline, Texas). Rock salt was chosen primarily for its relatively high reflecting power (which will be defined later). Of the crystals listed by Blokhin (1962, p. 231), those having the highest reflecting powers are aluminum, rock salt, lithium fluoride, quartz, and calcite. Their relative reflecting powers are, respectively, 140, 120, 110, 35 and 35. In addition, rock salt has a relatively small value of d (2.81 $\mathring{A}$), making the glancing angles larger and thus more convenient to work with. Moreover, it occurs in nature in large chunks which are fairly easily cleaved to the dimensions required for the geometry of Figure 1 (c).

The cleaved crystals measure about 1" by 0.8" in area and are mounted on a 6-foot diameter paraboloidal frame (as large as I felt could be launched without great difficulty). Incident radiation from a point source at infinity along the telescope's axis (the Z-axis) can be reflected while passing through a crystal if the Bragg condition (equation 1) is satisfied or very nearly satisfied. Thus any annular part of the lens is effective only over a narrow energy range, centered at

$$(4) \quad \bar{E}\ (\theta) = \frac{hc}{\bar{\lambda}} = \frac{hcn}{2d \sin \theta} = \frac{2.20n}{\sin \theta} \text{ KeV (for NaCl).}$$

The absorption length increases with energy, so the innermost crystals (those for which θ is smallest) are the thickest.

Because of its cubic structure, rock salt cleaves into parallelepipeds. Thus if salt crystals are mounted tangentially to a curve of slope

$$\frac{dz}{dy} = \begin{cases} -\tan\theta, & y \geq 0 \\ \tan\theta, & y \leq 0 \end{cases} \tag{5}$$

(where the axes are defined in Figure 3), one set of atomic planes will be at an angle θ relative to the telescope's axis. The angle of reflection must equal θ, the angle of incidence, so reflected x-rays leave the crystal at an angle 2θ relative to the Z-axis. In order for reflected x-rays to reach the focal point 0 (which is defined to be the origin of our co-ordinate system), the coordinates of the reflecting point P must therefore satisfy

$$\left|\frac{y}{z}\right| = \tan 2\theta. \tag{6}$$

Conditions 5 and 6 are satisfied by a parabola:

$$z(y) = z_o - \frac{y^2}{4z_o} = \frac{\mathcal{R}}{2} - \frac{y^2}{2\mathcal{R}} \tag{7}$$

where $\mathcal{R}$ is the radius of curvature in the limit $\left|\frac{y}{z}\right| << 1$. As for an ordinary parabolic mirror, z_o, the "focal length," is one-half the radius of curvature of the innermost part of the reflecting surface.

IV. THE LOW ENERGY LIMIT

Large balloons typically carry instrument packages to altitudes where the atmospheric pressure is between 2 and 4 millibars (i.e. only about 2 to 4 grams/cm^2 of air are above the detector). The transmission factor for vertically incident x-rays as a function of energy was calculated for pressures of 2, 3, and 4 mb in the following way.

The reduction in the intensity of a beam of x-rays of energy E as it passes through an infinitesimally thin layer of material with linear absorption coefficient μ is given by

$$dI = - I\mu \, |dz| \tag{8}$$

where $|dz|$ is the thickness of the layer. If the absorbing material consists of n components (e.g. nitrogen and oxygen) with mass absorption coefficients $(\mu/\rho)_i$ and densities ρ_i, then

$$\mu = \sum_{i=1}^{n} (\mu/\rho)_i \rho_i . \tag{9}$$

The coefficients $(\mu/\rho)_i$ depend on energy while the densities ρ_i are, in the case of the earth's atmosphere, functions of the altitude, z. The intensity decreases as z decreases, so

$$dI = I \sum_{i=1}^{n} (\mu/\rho)_i \rho_i(z) \, dz \tag{10}$$

which has the solution

$$I = I_o \, e^{- \int_z^\infty \sum_{i=1}^{n} (\mu/\rho)_i \rho_i} \tag{11}$$

At altitudes above 123,000 feet (i.e. at pressures less than 4 mb) the atmosphere is essentially isothermal at T = 258°K $\pm$ 20°K (Ney et al.,1964). Thus, noting that the pressure due to the ith component of the atmosphere above an altitude z is

(12) $P_i(z) = \int_z^\infty \rho_i g \, dz = \frac{\rho_i(z)\, RT}{M_i}$ (ideal gas law),

where R is the universal gas constant, M_i is the molecular weight of the ith component, and g is the acceleration due to gravity (essentially constant throughout the atmosphere), we find that

(13) $\rho_i(z) = \rho_i(z_o) e^{-\frac{z-z_o}{h_i}}$ ($z_o \geq$ 123,000 ft.)

and

(14) $I(z) = I_o e^{-\sum_{i=1}^{n} \rho_i(z_o)(\mu/\rho)_i h_i e^{-\frac{z-z_o}{h_i}}}$

where $h_i \equiv \frac{RT}{M_i g}$ is the scale height for the ith component of the atmosphere.

The percent composition by volume of air at 123,000 ft. was found by interpolating (graphically) values of the percent composition at various altitudes tabulated in the Handbook of Chemistry and Physics (Thirty First Edition, p. 2678). The calculations take into account the presence of argon as well as nitrogen and oxygen. (Although ρ_{Argon} is only $\sim$ 1/4% of ρ_{Air}), $(\mu/\rho)_{Argon} \cong 15 \cdot (\mu/\rho)_{Nitrogen}$ at low energies so argon's contribution to μ is not negligible.) The calculated atmospheric transmission for energies between 14 and 140 KeV is shown in Figure 4.

Atmospheric absorption, while never negligible, becomes very important at energies below 30 KeV. For a source spectrum which falls off as rapidly as the Crab's ($\frac{dN}{dE} \propto E^{-1.9}$ (Peterson, 1965)), the peak intensity of the observed flux occurs near 25 KeV (at 3.3 gm/cm^2 atmospheric depth).

V. THE REFLECTING POWER OF CRYSTALS

The reflecting power R of a crystal for x-rays of energy E is defined to be

$$R(E) \equiv \int \rho(\theta,E)\,d\theta \qquad (15)$$

where θ is the glancing angle in radius, ρ is the ratio of reflected to incident intensity, and the limits of integration include that range of θ over which reflection is appreciable. (For rock salt, $\Delta\theta$ (full width of ρ curve at half its maximum value) is on the order of 0.5°; for nearly perfect crystals such as calcite $\Delta\theta$ is only a few seconds.) Using a rotating crystal method, Bragg and others (1921) measured first order reflections from the faces (cleavage planes) of various thick crystals of rock salt at an energy of 20 KeV (rhodium Kα radiation), obtaining an average value $\bar{R}_B = 5.5 \times 10^{-4}$ (here the subscript B indicates the Bragg case of reflection from a thick crystal).

I made measurements of the reflecting power in the Laue case (through a crystal of optimum thickness) at higher energies, using a tungsten target x-ray machine at an anode potential of 50 kilovolts. The primary beam was collimated to about 0.1° (FWHM) but contained a broad, continuous spectrum of x-rays of energy up to 50 KeV. Figure 5 shows two energy spectra for x-rays from a tungsten target at 50 kilovolts. The lower curve was obtained by Ulrey (1918) using a high resolution (calcite crystal) x-ray spectrometer, while the upper curve is the spectrum I measured using a Harshaw Integral Line 1 inch diameter NaI (Tl) crystal and

photomultiplier tube assembly with a Victoreen PIP-400 pulse height analyzer. The resolution of the detector I used was relatively good for a sodium iodide crystal: resolution (FWHM) $\tilde{=}$ 25% at 28 KeV. The radiation from the target contained no line emissions since the tungsten Kα line occurs at 59 KeV.

The number of photons reflected per second by a crystal held at a fixed angle θ relative to the incident beam will be

$$(16) \qquad N'(\theta) = \int \frac{dN}{dE}(E)\ \rho(\theta,E)\ dE$$

where $\frac{dN}{dE}(E)$ is the incident differential number spectrum (photons sec^{-1} KeV^{-1}), E is the energy in KeV, and the range of integration includes that range of energy over which reflection is appreciable. The measured reflected spectrum was found to be sharply peaked at the Bragg energy, $E_B = \frac{2.20n}{\sin\theta}$ KeV, with a full width at half maximum not significantly greater than the FWHM resolution of the detector itself. Thus the energy range ΔE of the reflected x-rays is much less than E_B, so we can infer that ρ is a sharply peaked function of energy (for constant θ). So, provided $\frac{dN}{dE}(E)$ is slowly and predictably varying with energy at E_B (this is true for $E_B \tilde{<}$ 40 KeV for my measurements with a 50 kilovolt supply voltage), we can write

$$(17) \qquad N'(\theta) = \frac{dN}{dE}(E_B) \int \rho(\theta,E)\ dE.$$

As an alternate figure of merit for a crystal's reflecting power we can thus define a conveniently measureable "efficiency bandwidth product," E.B.:

$$(18) \qquad E.B.(\theta) \equiv \int \rho(\theta,E)\ dE = \frac{N'(\theta)}{\frac{dN}{dE}(E_B)}\ .$$

Using the measured value E.B. (θ) we can calculate R(E) from a simple relation which will be derived below.

I have also made measurements of R at the energies 22 KeV, 60 KeV, 88 KeV, and 121 KeV using radioactive sources (Cd-109, Am-241, Cd-109, and Co-57, respectively) in a Laue arrangement (Figure 6). Instead of narrowly collimating the monoenergetic x-rays from the source and rotating the crystal, I simply mounted the crystal in a plane midway between source and detector (which were a distance D = 40 inches apart) and let x-rays simultaneously impinge on the crystal over a sufficiently wide range of θ so that the power reflected to the detector (whose area is A_{Det}) was

$$(19) \qquad P'_{Det} = \int I_o \rho \, \Delta y \, dx$$

where I_o is the incident intensity at the position of the crystal, Δy is the height of the crystal, and x is the horizontal distance from centerline to reflecting point. For $E \gtrsim 22$ KeV ($\theta_B \lesssim .1$ rad), equation 19 becomes

$$(20) \quad P'_{Det} = I_o \ \Delta y \int \rho \frac{D}{2} \, d\theta = I_o \, \Delta y \, \frac{D}{2} \, R.$$

I_o was simply calculated from measurements of the intensity of radiation I_{Det} at the detector with the source turret pointed at the detector and the primary beam absorbers removed. For small θ, $I_o = 4I_{Det} = 4 \frac{P_{Det}}{A_{Det}}$ since the power falls off as the square of distance. Thus

$$(21) \qquad R = \frac{1}{2} \frac{P'_{Det}}{P_{Det}} \frac{A_{Det}}{D\Delta y}.$$

Source activities of about 1 millicurie were required to give a reflected intensity much greater than the background radiation detected by the 2 inch diameter sodium iodide crystal. The

background spectrum was peaked at 80 to 90 KeV, and seemed to be isotropic in the lab. Before lead shielding was put around the detector, the background counting rate was $\sim$ 6 counts/sec ($60 \leq E \leq 100$ KeV). A search through the Isotope Index (1963-64) revealed no 80-100 KeV x-ray emitters which were likely to be present in the walls of the building, so this radiation remains an unexplained nuisance.

The results of my measurements of R and E.B. will be presented in a later section. Some pertinent aspects of x-ray diffraction theory will first be discussed.

VI. THE KINEMATIC THEORY OF X-RAY DIFFRACTION

If a crystal is perfect (i.e. has no substitution or dislocation disorders) and if the crystal is so small that the intensity of x-rays is diminished only negligibly in passing through it, the reflected intensity is predicted accurately by the kinematic theory of x-ray diffraction (Zachariasen, 1945, pp. 82-110). Some results of this theory are summarized in the following paragraphs.

A perfect crystal of macroscopic size may be mathematically broken down into unit crystals, each of which has edges $\vec{a}_1$, $\vec{a}_2$, and $\vec{a}_3$ (which are not all coplanar). The amplitude of an x-ray scattered by a single loosely bound electron is given by the Thomson formula

$$E_e = \frac{e^2 \sin\phi}{mc^2 r} E_o \tag{22}$$

where ϕ is the angle between the incident electric field vector $\vec{E}_o$ and the propagation direction of the scattered radiation, and r is the distance from the scattering point to the observer. The amplitude scattered by a unit crystal is defined to be FE_e, where F is the "structure factor" of the unit crystal. F depends on the electron distribution in the unit crystal and on the directions of incident and scattered wave vectors. Since it includes a phase factor, F in general is complex.

If the dimensions of the macroscopic crystal are $N_1 a_1$, $N_2 a_2$, and $N_3 a_3$ (where N_1, N_2, and N_3 are each much greater than 1) the resulting diffraction pattern is very sharply peaked. The

diffracted intensity then is

$$(23)\quad I' = |F_B|^2 \prod_{i=1}^{3} \frac{\sin^2 N\pi(\vec{k}-\vec{k}_o)\cdot\vec{a}_i}{\sin^2 \pi(\vec{k}-\vec{k}_o)\cdot\vec{a}_i} \left(\frac{e^2 \sin\phi}{mc^2 r}\right)^2 I_o,$$

where $\vec{k}_o$ and $\vec{k}$ are the incident and scattered wave vectors, respectively, I_o is the incident intensity, and F_B is the value of F when the conditions for Braqq reflection from an atomic plane are satisfied or nearly satisfied.

The reflecting power $R_{perfect}$ is calculated from equation 23 by first expressing the reflected intensity I' in terms of the glancing angle (the angle between incident beam and reflecting planes) and the propagation direction of the reflected ray, and then integrating I' over solid angle and glancing angle. (The solid angle subtended by the detector is assumed to be large compared to the solid angle in which the reflected radiation is concentrated.) The result is

$$(24)\qquad R_{perfect} = Q_\theta \frac{t_o}{\cos\theta},$$

where t_o is the crystal thickness and

$$(25)\quad Q_\theta = \left(\frac{e^2}{mc^2}\right)^2 \frac{|F_B|^2}{V^2} \frac{1+\cos^2 2\theta}{2\sin 2\theta} \lambda^3$$

for unpolarized radiation. V is the volume of a unit crystal. If the glancing angle is held fixed but the energy of the radiation is allowed to vary a similar integration gives

$$(26)\qquad E.B._{perfect} = Q_E \frac{t_o}{\cos\theta}$$

where

$$(27)\quad Q_E = \left(\frac{e^2}{mc^2}\right)^2 \frac{|F_B|^2}{V^2} \frac{1+\cos^2 2\theta}{4\sin^2\theta} \frac{h^3c^3}{E}$$

for unpolarized radiation. For $\theta \lesssim .1$ radian

$$(28) \quad \text{E.B.}_{\text{perfect}} \cong R_{\text{perfect}} \frac{E}{\theta_B} .$$

The reflection from a perfect crystal of finite size is given more accurately by the results of the dynamic theory, which takes into account true absorption (which is due mainly to the photoelectric effect at energies below 150 KeV) and extinction (removal of energy from the primary beam by diffraction) in the crystal. But we are interested mainly in crystals with high reflecting powers. Single perfect crystals (even very small ones, with thicknesses of only a few thousand atomic planes) can reflect with efficiencies approaching unity but only over an extremely narrow range of glancing angle (or energy) so R and E.B. are very small for these crystals. On the other hand, a mosaic crystal consists of a large number of very small perfect crystal blocks at slightly differing orientations. Thus, for a mosaic crystal the bandwidth over which reflection occurs can be much larger than that for a single perfect crystal. The individual blocks of the mosaic crystal rock salt are small enough so that the kinematic theory can be applied to them individually, and we need not consider the dynamic theory here.

VII. THE REFLECTING POWER OF A MOSAIC CRYSTAL (LAUE CASE)

Zachariasen's (1945) derivations of expressions for the reflecting power of a mosaic crystal assume that the kinematic formulas apply to the individual blocks of the mosaic and that the distribution in orientation of perfect blocks (of average thickness t_o) within the mosaic can be described by a Gaussian function:

$$(29) \qquad W(\Delta) = \frac{1}{\sqrt{2\pi}\,\eta}\, e^{-\Delta^2/2\eta^2},$$

where Δ is "the magnitude of the angular deviation from the mean" and η is a constant for a particular mosaic crystal. The coupled differential equations for the incident beam power P_o and reflected beam power P_r as functions of the depth T into the crystal (measured normal to its surface) are, for the Laue case:

$$(30) \quad dP_o = -\mu_o P_o \frac{dT}{\cos\theta} - \sigma P_o\, dT + \sigma P_r\, dT$$

$$(31) \quad dP_r = -\mu_o P_r \frac{dT}{\cos\theta} + \sigma P_o\, dT - \sigma P_R\, dT$$

where μ_o is the ordinary linear absorption coefficient and σ is the probability of reflection per unit thickness of a thin layer of the mosaic crystal. The ratio of reflected to incident intensity for a mosaic of thickness T_o then becomes

$$(32) \quad \rho \equiv \frac{P_r(T_o)}{P_o(o)} = e^{-(\frac{\mu_o}{\cos\theta} + \sigma)T_o} \sinh(\sigma T_o)$$

$$(33) \quad \tilde{=} \sigma T_o e^{-(\mu_o/\cos\theta)T_o} \left[1 - \sigma T_o + \frac{2}{3}(\sigma T_o)^2 + \ldots\right],$$

where it was assumed $\sigma T_o \ll 1$. If only the first reflections of primary and reflected beams are taken into account (i.e. we

neglect the last terms in equations 30 and 31), the result is not very different from equation 33, if σT_o is small:

$$(34)\ \rho \equiv \frac{P_r(T_o)}{P_o(o)} \approx \sigma T_o\, e^{-\frac{\mu_o}{\cos\theta} T_o} \left[1 - \frac{\sigma T_o}{2} + \frac{\sigma^2 T_o^2}{6} + \ldots\right].$$

If the incident radiation is monoenergetic, we can calculate σ as a function of θ. We consider a small perfect crystal block whose reflecting planes have a normal unit vector $\hat{n}$ at a small angle Δ to the -y-axis: $\hat{n} = (\Delta_x, -\cos\Delta, \Delta_z) = (-\sin\Delta \sin\phi, -\cos\Delta, \sin\Delta\cos\phi)$, where $\Delta = \sqrt{\Delta_x^2 + \Delta_z^2}$ (see Fig. 7). Let the direction of the incident wave be described by a unit vector $\hat{u}_o = (0, \sin\theta, \cos\theta)$. We now express the distribution function in the symmetrical form

$$(35)\qquad W(\Delta_x,\Delta_z) = W_x(\Delta_x)\, W_z(\Delta_z)$$

$$(36)\qquad = g\, e^{-\pi g^2 \Delta_x^2}\ g\, e^{-\pi g^2 \Delta_z^2} = g^2 e^{-\pi g^2 \Delta^2}$$

which is normalized so that

$$(37)\qquad \int_{-\delta}^{\delta}\int_{-\delta}^{\delta} W(\Delta_x,\Delta_z)\, d\Delta_x\, d\Delta_z = 1.$$

(Here the integration limits include the values of Δ over which W is appreciable; for rock salt, $\delta \gtrsim 1°$ is sufficient.) Thus $W(\Delta_x,\Delta_z)\, d\Delta_x\, d\Delta_z$ is the probability that , in a thickness t_o of the mosaic, the incoming x-ray will strike a block whose normal is in the range $\Delta_x \pm \frac{d\Delta_x}{2}$, $\Delta_z \pm \frac{d\Delta_z}{2}$. Then the total intensity reflected in a thickness dT ($t_o \ll dT \ll \Lambda$) will be

$$(38)\ I_o\sigma(\theta)\, dT = I_o \int_{-\delta}^{\delta}\int_{-\delta}^{\delta} W(\Delta_x,\Delta_z)\, \frac{dT}{t_o}\, \varepsilon_p(\theta'-\theta_B)\, d\Delta_x\, d\Delta_z,$$

where θ is the mean glancing angle and $\varepsilon_p(\theta'-\theta_B)$ is the ratio of

reflected to incident intensity for a perfect crystal at an actual glancing angle θ' (the angle between $\hat{u}_o$ and the reflection planes of the block). From Fig. 7,

$$\sin\theta' = -\cos\alpha = -\hat{n}\cdot\hat{u}_o = \sin\theta\cos\Delta - \Delta_z\cos\theta \tag{39}$$

$$\tilde{=} \sin\theta - \Delta_z\cos\theta \tag{40}$$

$$\tilde{=} \sin\theta\cos\Delta_z - \cos\theta\sin\Delta_z \tag{41}$$

$$= \sin(\theta-\Delta_z).$$

Since Δ is a very small angle, we can accordingly write

$$\theta' = \theta - \Delta_z \tag{42}$$

so that

$$\sigma(\theta)\,dT = q^2\,\frac{dT}{t_o}\int_{-\delta}^{\delta} e^{-\pi q^2\Delta_x^2}\,d\Delta_x \int_{-\delta}^{\delta} e^{-\pi q^2\Delta_z^2}\,\mathcal{E}_p(\theta-\Delta_z-\theta_B)\,d\Delta_z. \tag{43}$$

$\mathcal{E}_p$ is very sharply peaked at $\theta' = \theta_B$, so it may be considered a δ - function normalized to $R_{perfect}$. Thus we obtain

$$\sigma(\theta)\,dT = \frac{dT}{t_o}\,R_{perfect}\,q\,e^{-\pi q^2(\theta_B-\theta)^2} \tag{44}$$

$$= W_z\,(\theta_B-\theta)\,\Omega\,\frac{dT}{\cos\theta}\;.*\dagger \tag{45}$$

$$\int\sigma T_o\,d\theta = \int\frac{W_z\,\Omega\,T_o}{\cos\theta}\,d\Delta_z = \Omega\,\frac{T_o}{\cos\theta} \tag{46}$$

and

$$\int(\sigma T_o)^2\,d\theta = \frac{\Omega^2 T_o^2}{\cos^2\theta}\int W_z^2\,d\Delta_z = \frac{q\,\Omega^2\,T_o^2}{\cos^2\theta} \tag{47}$$

so that we obtain from the first two terms of equation 33

$$R_{mosaic,Laue}(T_o) \equiv \int\rho\,d\theta \tilde{=} \frac{\Omega T_o}{\cos\theta}\,e^{-(\mu_o+q\Omega)\,\frac{T_o}{\cos\theta}}, \tag{48}$$

---

*Zachariasen (1945) uses the symbol $W(\Delta)$ not only for the function defined in equation 29, but also in place of the function W_z in equation 45.

†For brevity, we write $\Omega = \Omega_\theta$.

assuming $\sigma T_o << 1$.

The maximum reflecting power R obtainable in the Laue case will occur for the thickness $T_{o_{opt}}$ satisfying $\frac{dR}{dT_o} = 0$. This gives

$$T_{o_{opt}} = \frac{\cos\theta}{\mu_o + q\,\Omega} \tag{49}$$

and

$$R(T_{o_{opt}}) = \frac{\Omega}{\mu_o + q\,\Omega}\ e^{-1}. \tag{50}$$

A crystal having a value of q much less than $\frac{\mu_o}{\Omega}$ would be "ideally imperfect;" the Laue reflecting power of an ideally imperfect crystal of optimum thickness would be $\frac{\Omega}{\mu_o}\ e^{-1}$.

If the incident x-rays are not monoenergetic, but θ is fixed, σ may be calculated as a function of a variable $\Delta E \equiv E - E_B << E$ where E_B is the energy at which the Bragg condition is satisfied for a glancing angle θ. Then one obtains

$$\sigma(\Delta E) = E.B._{perfect}\ W_z\ (\Delta\theta_B(\Delta E))\ \left|\frac{d\theta_B}{dE}\right|\ \frac{1}{\cos\theta} \tag{51}$$

from which we calculate

$$E.B._{mosaic,Laue} = \int \sinh \sigma(\Delta E)\ T_o e^{-(\mu_o + \sigma(\Delta E))T_o}\ d(\Delta E). \tag{52}$$

We again assume $\sigma T_o << 1$ and make a Taylor's expansion of the integrand, obtaining

$$E.B._{mosaic,Laue} = \left[e^{-(\mu_o + q\ E.B._{perfect}\ \frac{\theta_B}{E})\frac{T_o}{\cos\theta}}\right] \times \frac{E.B._{perfect}\ T_o}{\cos\theta} \tag{53}$$

$$= R_{mosaic,Laue}\ \frac{E}{\theta_B}\ . \tag{54}$$

Referring back to Figure 2, we can compare the optimum Laue case reflecting power with the maximum reflecting power that would

be obtainable in the Bragg case. Since the probability of reflection is proportional to crystal volume (for an infinitesimal crystal) and the attenuation of incident or refelcted photons (which have the same energy) is $e^{-\mu \cdot \text{ path length}}$ (where μ is an effective absorption coefficient which includes the power loss due to diffraction), we have for the reflected intensity I' in the Laue and Bragg cases, respectively, the following relations:

$$(55) \qquad dI'_L = cI_o \, e^{-\mu \frac{T_o}{\cos \theta}} \, dx$$

$$(56) \qquad dI'_B = cI_o \, e^{-\mu \frac{2x}{\cos \theta}} \, dx$$

so the ratio of maximum reflected intensities is

$$(57) \qquad \frac{I_L' \text{ max}}{I_B' \text{ max}} = \frac{cI_o \int_o^{T_{o_{opt}}} e^{-\mu \, T_{o_{opt}}/\cos\theta} \, dx}{cI_o \int_o^{\infty} e^{-\mu \, 2x/\cos\theta} \, dx} = \frac{2}{e} \approx 74\%$$

(where $T_{o_{opt}} = \frac{\cos \theta}{\mu}$). If a crystal of thickness $\frac{\cos \theta}{\mu}$ is used in the Bragg case as well as the Laue case, the ratio becomes 85%. Thus the Laue case is not only much more convenient to use in the lens; it is also nearly as efficient as Bragg geometry could be.

In a recent paper, Zachariasen (1967 a) states the results of his new general theory of x-ray diffraction in real crystals. This theory takes into account primary extinction (extinction within an individual perfect block) as well as secondary extinction (in the crystal as a whole) and ordinary absorption. In the notation I have been using, the new formulae can be writted as follows (for the Laue case):

$$R = \frac{Q\,T_o}{\cos\theta}\; e^{-\mu_o \frac{T_o}{\cos\theta}}\; y, \tag{58}$$

$$y = \frac{1}{\sqrt{3x}} \sinh \sqrt{3x}, \tag{59}$$

$$x = \alpha\, Q \left\{ \bar{t} + (T-\bar{t}) \left[1 + \left(\frac{\alpha}{g}\right)^2\right]^{-1/2} \right\}, \tag{60}$$

$$\alpha = \frac{2\bar{t}_\perp}{3\lambda}, \tag{61}$$

where $\bar{T}$ is the mean path length through the crystal, $\bar{t}$ is the mean path length through a perfect crystal domain, and $\bar{t}_\perp$ is the mean thickness of the perfect domain measured normal to the incident beam in the plane of incidence (the plane containing incident and reflected wave vectors). According to Zachariasen (1967 b),

$$y = \frac{1}{\sqrt{1 + 2x}} \tag{62}$$

is a slightly better expression than equation 59 for most crystals. (The expansion of $\frac{1}{\sqrt{1 + 2x}}$, for small x, lies between the expansion of equation 59 and the expansion of $\frac{1}{\sqrt{3x}} \tan^{-1}\sqrt{3x}$ (which Zachariasen (1967 a) recommended in place of equation 59 for crystals with x and $\mu\bar{T}$ greater than one.))

If the perfect domains can be considered as spheres of radius r, and if $r << T_o$, equation 60 becomes

$$x = \frac{Q}{\lambda} \left\{ \frac{3}{2} r^2 + \frac{T_o}{\cos\theta} \frac{\lambda g}{\sqrt{1+(\lambda g/r)^2}} \right\} \tag{63}$$

$$\simeq \frac{Q\,T_o\,g}{\cos\theta} \left[1 + \left(\frac{\lambda g}{r}\right)^2\right]^{-1/2} \tag{64}$$

if r is very small. (When r is so small, primary extinciton is negligible.) If we assume that $x << 1$ for our crystal, then a

Taylor's expansion gives

$$y \simeq 1 - x \tag{65}$$

so

$$R \simeq \frac{QT_o}{\cos\theta}\, e^{-\mu_o T_o/\cos\theta}\left[1 - \frac{T_o}{\cos\theta}\,\frac{qQ}{\sqrt{1+(\lambda g/r)^2}}\right] \tag{66}$$

$$\simeq \frac{QT_o}{\cos\theta}\, e^{-(\mu_o + gQ/\sqrt{1+(\lambda g/r)^2})\, T_o/\cos\theta}. \tag{67}$$

If we are concerned with energies so high that $\lambda \ll r/g$, then equation 67 reduces to the result obtained earlier (equation 48). The validity of the assumptions made here will be demonstrated when we compare theoretical and experimental values of R for natural rock salt in the energy range 20-140 KeV.

VIII. THEORETICAL AND MEASURED VALUES OF R AND $T_{\circ opt}$

Using equation 50, I calculated the reflecting power R of rock salt crystals of optimum thickness in the Laue case. In calculating Q, I took values of $|F|$ (for first and second order reflections from NaCl) from a graph given by James (1948). James' graph shows theoretical values (calculated from the Hartree theory) and experimental values (which are in good agreement with the theory). For first order reflections from cleavage planes $|F| \tilde{=} 21.3$, while for second order reflections $|F| \tilde{=} 12.8$ (these values apply to a unit crystal containing one sodium and one chlorine atom). X-ray diffraction theory does not predict a value of g, but measurements of the reflecting power (in the Laue case) at different thicknesses of the same crystal yield a value of g. Zachariasen (1945, p. 168) suggests for rock salt $g \tilde{=} 260$. Values of $\frac{\mu}{\rho}$ (where ρ is the density) for sodium and chlorine were found in the Handbook of Chemistry and Physics; from them, we calculate the ordinary linear absorption coefficient for sodium chloride

$$\mu_\circ = \left(\frac{\mu}{\rho}\right)_{Na} \rho_{Na} + \left(\frac{\mu}{\rho}\right)_{Cl} \rho_{Cl} \tag{68}$$

and the ordinary absorption length

$$\Lambda_\circ \equiv \frac{1}{\mu_\circ} , \tag{69}$$

which are shown, as functions of energy, in Figs. 8 and 9.

The first and second order theoretical curves of R labeled g = 260 in Fig. 10 were calculated from equation 50. Although

$\frac{g\,Q\,T_o}{\cos\theta} \sim 0.3$ near the peak of the first-order curve, equation 48 (which assumed $\frac{g\,Q\,T_o}{\cos} << 1$) still agrees very well with the following formula, obtained by integrating a Taylor's expansion of equation 32 about $\sigma T_o = 0.3$:

$$(70)\quad R = e^{-\mu_o\ T_o/\cos\theta}\left[0.964\ \frac{Q\,T_o}{\cos\theta} - 0.741\ \left(\frac{Q\,T_o}{\cos\theta}\right)^2\right].$$

The "ideally imperfect" first order curve of Fig. 10 represents the upper limit (attained when $g = 0$) on R_{Laue} for rock salt. The above values of $|F|$ and g were also used to calculate the theoretical optimum thickness. Equation 50 gave the curves shown in Fig. 11.

The experimental points of Fig. 10 represent the values of R which I obtained from my machine data (filled-in circles) and source data (open circles) for rock salt crystals of optimum thickness (determined experimentally). Each machine point is an average of as many as eight values of R (calculated from the efficiency bandwidth products measured at a given energy). The two experimental values of optimum thickness shown in Fig. 11 were obtained by measuring relative reflecting power (using sources) as a function of crystal thickness at 22 KeV and 60 KeV. Approximately ten measurements with crystals of various thicknesses (all close to the theoretical optimum thickness) were made at each of the two energies.

Within the limits of experimental error, the measured values of R and optimum thickness are in good agreement with the values predicted by equations 50 and 49. Some of the machine measurements of R may have tended to be high because the incident beam was

very narrow (half the intensity was confined within an area of only 0.007 cm^2 at the crystal). Conceivably, a region this small could have an anomalously low value of g, thus permitting a larger value of R. In fact, the distribution function $W(\Delta)$ may be significantly non-Gaussian over much small areas, so that the definition of g (equations 35 and 36) and the formulas for optimum thickness and reflecting power (equations 49 and 50) given above do not apply.

Consider, for example, a hypothetical small mosaic crystal whose distribution function falls off linearly with Δ_x and Δ_z:

$$(71)\quad W(\Delta_x,\Delta_z) = \begin{cases} \gamma(\Delta_o-|\Delta_x|)(\Delta_o-|\Delta_z|), & |\Delta_x|\leq \Delta_o \text{ and } |\Delta_z|\leq\Delta_o \\ 0, & |\Delta_x|>\Delta_o \text{ or } |\Delta_z|>\Delta_o. \end{cases}$$

Then normalization (equation 37, with $\delta \geq \Delta_o$) requires

$$(72)\qquad \gamma = \frac{1}{\Delta_o^4}\ .$$

As before, we calculate for $\sigma(\theta)$ (using equation 38)

$$(73)\quad \sigma(\theta) = \frac{R_p}{t_o}\ W_z\ (\theta-\theta_B) = \frac{Q}{\cos\theta}\ W_z\ (\theta-\theta_B)$$

where now

$$(74)\quad W_z\ (\theta-\theta_B) = \frac{1}{\Delta_o^2}\ (\Delta_o-|\theta-\theta_B|).$$

In place of equation 47, we obtain

$$(75)\quad \int(\sigma T_o)^2\ d\theta = \frac{2}{3\Delta_o}\ \frac{Q^2T_o^2}{\cos^2\theta}$$

so that the formula for R (eq. 48) is still valid if q is set equal to $\frac{2}{3\Delta_o}$.

Clearly, other non-Gaussian distribution functions will give rise to the same formula (eq. 48) for R, provided $\sigma T_o << 1$. Thus,

although the value of q can be determined from measurements of R at more than one energy, these measurements tell us nothing of the actual form of the distribution function W.

IX. CONSTRUCTION DETAILS

The above calculations of the reflecting power R(E) can be used to determine the effective area of the lens as a function of energy for a given lens geometry. Some comments on the geometry and construction of this lens are therefore in order.

Reflecting crystals can be mounted in any array such that equations 5 and 6 are approximately satisfied everywhere in the crystal array. (For crystals of finite dimensions, these equations cannot be exactly and simultaneously satisfied at all possible reflecting points; but if the individual crystals are small enough (smaller than the detector) and well enough aligned, and if the x-ray source is at a small enough angle to the telescope's axis, then all the reflected x-rays will hit the detector (i.e. the geometry is 100% efficient under these conditions)). (The actual angular response function will be dealt with in a later section.) It seemed simplest to use the continuous curve satisfying equations 5 and 6 (i.e. a parabola) to define the surface on which the crystals would be mounted.

The parabola's focal length f was chosen to be 114.6 inches. This puts all the reflecting crystals approximately 114.6 inches away from the detector (since θ_{max} is small). Thus an incident x-ray from an angle $\epsilon = 1°$ off the telescope's axis will, after reflected, miss the focal point by about $f\epsilon$ = 114.6" x 1° x $\frac{1 \text{ rad.}}{57.3°}$ = 2". So with a 2 inch diameter detector centered at the focal point, the field of view is a cone with a semi-vertex angle

of 1°, provided that the crystals are infinitesimally small and perfectly tangent to the paraboloid. Using crystals about 0.8" by 1.0" in area makes the collection efficiency drop off gradually at smaller off-axis angles. As will be shown later, the efficiency is down to 50% at $\epsilon \tilde{=} 0.5°$ for the focal length, crystal size, and detector size of this telescope.

Decreasing the size of the crystals significantly would increase the time spent cleaving crystals. Furthermore, to take advantage of the smaller crystal size, the angular tolerances of the frame would have to be reduced below $\pm$ 1/4° -- accuracy which is quite difficult to attain in practice. Moreover, for rock salt the reflected beam's direction may vary by perhaps $\pm$ 1/4°, because of the mosaic structure.

It was thus decided to mount the reflecting crystals on a frame consisting of 36 concentric circular bands (in 1 inch radial increments) inserted into 24 radial ribs or "spokes" (see Figure 12), each of which has 36 slots. The depth of the slots increases parabolically with increasing distance from the telescope's axis. The bottom of each slot is defined by a jig-bored hole. According to the foreman of the machine shop which did this work, this technique permitted the bottoms of the slots to be defined (relative to a spoke's bottom edge) to an accuracy of $\pm$ .001". The bands are .050" thick cold rold round edge flat wire, .500" wide and selected out of stock for uniformity in width to $\pm$ .001". The bands are silver soldered together (after

being rolled to the correct radius of curvature) and are epoxied into the slots with a highly thixotropic (non-running) epoxy. Between each pair of spokes, a thin skin of Silkspan paper is applied across all the bands. The Silkspan is applied wet, with butyrate dope to make it adhere to the tops of all bands. On drying, the Silkspan shrinks to a tight skin on which the salt crystals can be glued. Figure 13 is a photograph of the partially completed frame with Silkspan covering one of its sectors.

The crystals were cleaved from chunks up to several cubic inches in size. A hammer and sharp chisel were used in the first stage of cleaving. Then crystals of intermediate thicknesses were obtained by successively cleaving with a hammer and an ordinary single edge razor blade. The thinnest crystals were cleaved by gently pushing the razor blade along a cleavage plane. Crystals larger than a square inch in area but thinner than .030" could be obtained in this way. Fig. 14 is a photograph of various cleaved crystals and one of the larger "raw" chunks.

X. THE GAIN OF THE TELESCOPE

We define the effective area of the lens at some energy E in the following way:

$$(76)\quad A_{lens}(E) \equiv \frac{\text{rate at which reflected x-rays are detected}}{\text{intensity incident on lens (photons sec}^{-1}\text{)}} \cdot \frac{\text{(photons sec}^{-1}\text{)}}{\text{(unit area normal to beam)}^{-1}\text{)}} \cdot$$

If the ith crystal of the lens has area A_i and is inclined at an angle θ_i, and if all reflected x-rays impinge on the detector, then we can write for the effective area of the lens

$$(77)\quad A_{lens}(E) = \sum_{i=1}^{N} \rho_i(\theta_i,E)\, A_i \cos\theta_i$$

where ρ_i is the ratio of reflected to incident intensity for the ith crystal and N is the number of crystals making up the lens. The shape of the function $\rho(\theta)$ for rock salt at a given energy may vary greatly among different crystals (Bragg, 1914), so the subscript i must be retained on ρ. (Nevertheless, the reflecting power, $R = \int \rho\, d\theta$, is nearly the same for all the crystals.)

In the case of this lens, each crystal has the same area, A_c. To evaluate the summation

$$(78)\quad S = \sum_{i=1}^{N} \rho_i(\theta_i,E) \cos\theta_i$$

we note the following properties of the lens. First, there is a large number of crystals per annulus, and the angular difference between adjacent annular arrays is only 0.3°. Secondly, there are irregularities in the lens frame (limited to $\pm$ 1/4°), so that the total probability of a crystal being inclined at angle θ is a smooth function of θ. (Figure 15 illustrates qualitatively how

Gaussian-like probability distributions p_i and p_{i+1} centered at Θ_i and Θ_{i+1} (the nominal inclinations of the i$\underline{\text{th}}$ and i + 1$\underline{\text{st}}$ annular arrays) can add up to a total probability distribution P_T which is relatively constant between Θ_i and Θ_{i+1}.)

Thus there will be a number $\Delta N >> 1$ of crystals with angles of inclination throughout the range $\theta \pm \frac{\Delta\theta}{2}$, where $\Delta\theta = 0.3° << \theta$. Equivalently, we can say there will be ΔN crystals at the Bragg angle for energies in the range $E_B \pm \frac{\Delta E}{2}$, where $\Delta E = \Delta\theta \left|\frac{dE_B}{d\theta}\right| \simeq \frac{\Delta\theta}{\theta} E$. The average value of S in this energy range is

$$(79)\quad \bar{S}(E) = \frac{1}{\Delta E} \int_{E-\frac{\Delta E}{2}}^{E+\frac{\Delta E}{2}} \sum_{i=1}^{N} \rho_i(\theta_i, E) \cos\theta_i \, dE$$

$$(80)\quad = \frac{\Delta N}{\Delta E} E.B. \cos\theta_B$$

since ΔN of the $\rho_i(\theta_i,E)$ curves are centered within the given energy interval (see Fig. 16). Moreover, the $\rho_i(\theta_i,E)$ curves for natural rock salt have widths on the order of ΔE, so that S(E) does not fluctuate appreciably in the energy range $E \pm \frac{\Delta E}{2}$. (Even if fluctuations in S did occur over an energy interval as small as a few KeV, the telescope's response would be smoothed by the relatively broad energy resolution of the sodium iodide detector.) Thus we can equate S(E) to its average value in the given energy range, and we obtain:

$$(81)\quad A_{lens}(E) = A_c \frac{\Delta N}{\Delta E} E.B. \cos\theta_B$$

Assuming that the reflecting crystals completely cover the paraboloid, $A_c \Delta N$ is the geometrical area on the paraboloid where crystals can reflect x-rays in the energy range $E \pm \frac{\Delta E}{2}$. We can write

$$(82) \qquad \frac{A_c \Delta N}{\Delta E} = \frac{dA}{dE}$$

$$(83) \qquad = \frac{dA}{d\theta} \left|\frac{d\theta_B}{dE}\right|$$

$$(84) \qquad \simeq 2\pi R \sin\theta_B R \frac{\theta_B}{E} = 2\pi R^2 \sin\theta_B \frac{\theta_B}{E}.$$

Thus we finally obtain

$$(85) \quad A_{lens}(E) = 2\pi R^2 \sin\theta_B \frac{\theta_B}{E} R \frac{E}{\theta_B} \cos\theta_B = \pi R^2 R \sin 2\theta_B.$$

For this lens, R = 229.2 inches so the contribution to A_{lens} resulting from nth order reflections at a given energy becomes

$$(86) \quad A_{lens}(E,n) \simeq 72.7 \times 10^4 \frac{nR}{E(KeV)} \text{ in}^2 .$$

Here R is evaluated for the appropriate order of reflection (n) and for the actual thickness of the crystals which are in a position to produce nth order reflections at energy E.

Since the second-order reflecting power, R_{II}, is only about one-fifth of R_I, the thickness of the reflecting crystals was chosen to be equal to the first-order optimum thickness for most of the lens. It was, however, decided to design the outermost part of the lens for second-order reflections between 28 and 40 KeV instead of first order reflections between 14 and 20 KeV. The principal reason for this modification is the realization of how strong atmospheric absorption is at these energies (see Fig. 4). Additional reasons are the increased difficulty of cleaving crystals to thicknesses less than .024" and the fact that the reflecting power itself is dropping off fairly rapidly at energies below 30 KeV. (At 15 KeV, R is only about 60% of its maximum

value, according to the theoretical curve (q = 260) of Figure 10. Moreover, at energies below 20 KeV, primary extinction (which will be mentioned again later) makes the actual value of R less than the value predicted by the theory I have discussed.)

Using the theoretical (q = 260) curves for R and defining the telescope's gain to be

$$G = \frac{A_{lens} + A_{detector}}{A_{detector}} \tag{87}$$

we obtain the curve shown in Fig. 17. This curve takes into account first-order and second-order reflections for all θ between 0.96° and 8.81°.

Provided that the lens increases the signal (i.e. counting rate due to x-rays from a celestial source) without increasing the background noise (i.e. leakage through shielding and/or anticoincidence detectors and isotropic x-rays entering through the telescope's forward aperture), the minimum intensity detectable (at 3σ or any other confidence level) is lowered by a factor of G when the lens is put above the conventional detector. Since the field of view of this telescope is so small, the contribution of focused isotropic x-rays (atmospheric or extraterrestrial) to the background should be very small. (By erecting cylindrical collimators above the flat wire bands (as suggested in Fig. 3) isotropic x-rays can also be prevented from directly reaching the central detector.)

XI. THE ANGULAR RESPONSE OF THE TELESCOPE

The gain curve calculated above assumes that all reflected x-rays strike the detector; that is, the boundaries of the reflected beam in the Z = 0 plane are assumed to satisfy $\sqrt{x^2+y^2}$ < radius of detector. This condition is satisfied if the reflecting crystals are sufficiently small and the incident x-rays come from a direction sufficiently close to the telescope's axis. The dependence of focusing efficiency, $\mathcal{E}$, on the off-axis angle, ϵ, will now be calculated.

We first consider a reflecting crystal of infinitesimal dimensions lying on and tangent to the paraboloid. For convenience, we take the reflecting point P to lie over the y-axis (see Fig. 18). The incident and reflected rays (whose propagation directions are the unit vectors $-\hat{v}_1$ and $\hat{v}_2$, respectively) must satisfy the law of reflection

$$\hat{v}_2 \times \hat{n} = \hat{n} \times \hat{v}_1 \tag{88}$$

where $\hat{n}$ is a unit vector perpendicular to the reflecting plane: $\hat{n} = -\cos\theta\,\hat{j} + \sin\theta\hat{k}$. This gives $\hat{v}_2$ as a function of $\hat{v}_1$ and θ, and we find the coordinates (x_I, y_I) of the point I at which the reflected ray hits the detector (the z=0 plane) from the following relations:

$$\frac{v_{2x}}{v_{2z}} = \frac{x_I - 0}{0 - z} \tag{89}$$

$$\frac{v_{2y}}{v_{2z}} = \frac{y_I - Y}{0 - z} \quad . \tag{90}$$

The exact results are

$$(91)\quad x_I = -\frac{v_{1x}}{(v_{1y}\sin 2\theta + \sqrt{1-v_{1x}^2-v_{1y}^2}\cos 2\theta)}\ \frac{\mathcal{R}}{2}\left[1-\tan^2\theta\right]$$

$$(92)\quad y_I = -\frac{\sqrt{1-v_{1x}^2-v_{1y}^2}\sin 2\theta - v_{1y}\cos 2\theta}{\sqrt{1-v_{1x}^2-v_{1y}^2}\cos 2\theta + v_{1y}\sin 2\theta}\ \frac{\mathcal{R}}{2}\left[1-\tan^2\theta\right] + 2\mathcal{R}\frac{\sin^2\theta}{\sin 2\theta}.$$

If we denote by ϵ the angle between the z-axis and $\hat{v}_1$, and if ϵ is small, we can write

$$(93)\qquad v_{1z} = \cos\epsilon \tilde{=} 1 - \frac{\epsilon^2}{2}$$

$$(94)\qquad v_{1x} = \sin\epsilon_x \tilde{=} \epsilon_x$$

$$(95)\qquad v_{1y} = \sin\epsilon_y \tilde{=} \epsilon_y.$$

For this telescope, $\epsilon < .02$ radians for all focused x-rays, so the following are very good approximations:

$$(96)\quad x_I = -\frac{\epsilon_x}{\epsilon_y\sin 2\theta + \cos 2\theta}\ \frac{\mathcal{R}}{2}\left[1-\tan^2\theta\right]$$

$$(97)\quad y_I = -\frac{(\sin 2\theta - \epsilon_y\cos 2\theta)}{\cos 2\theta + \epsilon_y\sin 2\theta}\ \frac{\mathcal{R}}{2}\left[1-\tan^2\theta\right] + 2\mathcal{R}\frac{\sin^2\theta}{\sin 2\theta}.$$

Consider now an x-ray source at infinity in the x-z plane (so $\epsilon_x = \epsilon$ and $\epsilon_y = 0$). Let x-rays from it be reflected at a point P' on the paraboloid above the y' axis, which is at an angle ϕ to the y-axis (see Fig. 19). Transforming coordinates leads to

$$(98)\quad x_I(\epsilon,\phi) = \frac{\mathcal{R}}{2}\left[1-\tan^2\theta\right]\frac{-\epsilon\cos^2 2\phi + \sin 2\theta\sin\phi + \epsilon\cos 2\theta\sin^2\phi}{\cos 2\theta - \epsilon\sin\phi\sin 2\theta} - 2\mathcal{R}\frac{\sin^2\theta\sin\phi}{\sin 2\theta}.$$

$$(99)\quad y_I(\epsilon,\phi) = \frac{\mathcal{R}}{2}\left[1-\tan^2\theta\right]\frac{-\epsilon\cos\phi\sin\phi - \sin 2\theta\cos\phi - \epsilon\cos 2\theta\sin\phi\cos\phi}{\cos 2\theta - \epsilon\sin\phi\sin 2\theta} + 2\mathcal{R}\frac{\sin^2\theta\cos\phi}{\sin 2\theta}.$$

For $\theta << \frac{\pi}{2}$, these become

$$(100)\quad x_I \tilde{=} \mathcal{R}\epsilon \frac{\tan\theta}{\tan 2\theta}(\sin^2\phi - \cos^2\phi) \tilde{=} -\frac{\mathcal{R}\epsilon}{2}\cos 2\phi$$

$$(101)\quad y_I \tilde{=} \mathcal{R}\epsilon \frac{\tan\theta}{\tan 2\theta}(-2\sin\phi\cos\phi) \tilde{=} -\frac{\mathcal{R}\epsilon}{2}\sin\phi.$$

Thus the reflected x-rays fall close to a circle of radius $\frac{\mathcal{R}\epsilon}{2}$ in the detector plane, provided all the reflecting crystals are of infinitesimal size.

Accordingly, in applications where convergence of reflected x-rays to a point is desired even for $\epsilon > 0$ (e.g. focusing to a photographic film or an array of small, independent scintillation detectors in the z=0 plane), this x-ray lens could not be used satisfactorily. A parabolic array of crystals under the detector (the geometry of Fig. 1(a)) would, however, give convergence.

A focusing x-ray telescope lens must consist of reflecting crystals having finite dimensions (unless a continuously bent crystal is used). Then the formulas given above for (x_I, y_I) apply only to the center of a spot in the x-y plane "illuminated" by x-rays reflected from a crystal centered at P'. If the projection of a reflecting crystal on the x-y plane is a rectangle of dimensions a(in the azimuthal direction) by b (in the radial direction), we can write the coordinates of the vertices of the rectangle which is the boundary of a reflected beam in the x-y plane (see Fig. 20):

$$(102)\quad v_{1x} = x_I - \ell\sin(\phi+\delta),\quad v_{1y} = y_I + \ell\cos(\phi+\delta)$$

$$(103)\quad v_{2x} = x_I - \ell\sin(\phi-\delta),\quad v_{2y} = y_I + \ell\cos(\phi-\delta)$$

$$(104)\quad v_{3x} = x_I + \ell \sin(\phi+\delta), \quad v_{3y} = y_I - \ell \cos(\phi+\delta)$$

$$(105)\quad v_{4x} = x_I + \ell \sin(\phi-\delta), \quad v_{4y} = y_I - \ell \cos(\phi-\delta)$$

where ϕ is the angle from the y-axis to the y' axis (the y' axis passes under P', the center of the reflecting crystal), $\ell = \frac{1}{2}\sqrt{a^2+b^2}$, and $\delta = \tan^{-1}\left(\frac{a}{b}\right)$.

Determining the positions of these vertices is the first step in a series of calculations (performed by computer) which finally yield the collection efficiency, $\mathcal{E}$. Those vertices which lie inside the detector's boundary (i.e. those which satisfy

$$(106)\quad v_{ix}^2 + v_{iy}^2 < (\text{radius of detector})^2)$$

are labeled $\vec{VI}_i$ and are stored separately from the vertices $\vec{VO}_i$ which lie outside the detector's boundary. The number of vertices inside the boundary is counted; this number is N.

The computer next finds the points of intersection (if any) between the detector's boundary and the rectangle whose vertices have just been calculated. These points are labeled $\vec{I}_i$ and are counted (there are M of them).

In calculating the mutual area A_m which is contained by both the rectangle and the detector boundaries, the formula for the area A_{Ac} bounded by an arc of radius R and a chord of length L is useful:

$$(107)\quad A_{Ac} = R^2 \sin^{-1}\left(\frac{L}{2R}\right) - \frac{L}{4}\sqrt{4R^2-L^2}\ .$$

This formula, along with the usual area formulas for triangles,

rectangles, and trapezoids, leads to the formulas for A_m given in Table I (here R is R_D, the radius of the detector's boundary). The formula to be used in a given case depends on N and M, the seven possible combinations of which are illustrated in Fig. 21.

Table I

N	M	A_m	
0	0	0	
0	2	A_{Ac}	where $L = \lvert\vec{I}_1 - \vec{I}_2\rvert$
1	2	$A_{Ac} + \frac{S_1 S_2}{2}$	where $L = \lvert\vec{I}_1 - \vec{I}_2\rvert$, $S_1 = \lvert\vec{VI}_1 - \vec{I}_1\rvert$, $S_2 = \lvert\vec{VI}_1 - \vec{I}_2\rvert$
2	2	$A_{Ac} + \frac{S_1+S_2}{2} \lvert\vec{VI}_1 - \vec{VI}_2\rvert$	where $L = \lvert\vec{I}_1 - \vec{I}_2\rvert$, $S_1 = \min\{\lvert\vec{VI}_1 - \vec{I}_1\rvert, \lvert\vec{VI}_2 - \vec{I}_1\rvert\}$, $S_2 = \min\{\lvert\vec{VI}_1 - \vec{I}_2\rvert, \lvert\vec{VI}_2 - \vec{I}_2\rvert\}$
2	4	ab	(an approximation, but this case is rare)
3	2	$ab - \frac{1}{2} \lvert\vec{VO}_1 - \vec{I}_1\rvert \lvert\vec{VO}_1 - \vec{I}_2\rvert + A_{Ac}$	where $L = \lvert\vec{I}_1 - \vec{I}_2\rvert$
4	0	ab	

The above calculations of A_m were made by the computer (using the exact equations 98 and 99 for x_I and y_I) for each of the η crystals comprising an annulus. The collection efficiency $\mathcal{E}$ for that annulus at a given off-axis angle ϵ is defined to be the fraction of total reflected beam area which is intercepted by the detector:

(108) $$\mathcal{E}(\theta,\epsilon) \equiv \frac{\Sigma A_m}{\eta ab} \quad .$$

Values of $\mathcal{E}$ were computed for 11 annuli ($.86° \leq \theta \leq 8.81°$) at values of ϵ ranging from 0.00° to 0.90° in steps of 0.05°. Curves of $\mathcal{E}(\epsilon)$ for the innermost and outermost annuli are shown in Fig. 22. The calculations assume a = 0.8", b = 1.0", and R_D (the radius of the detector) = 1.0". To a good approximation, the opening half angle (the value of ϵ at which $\mathcal{E} = 0.5$) is just

(109) $$\epsilon_{1/2} \doteq \frac{\text{radius of detector boundary}}{\text{focal length of lens}} = \frac{2R_D}{\mathcal{R}} = 0.50°,$$

since for $\epsilon = \frac{2R_D}{\mathcal{R}}$ the center of the reflected beam will fall close to a circle (in the detector's plane) of radius $\frac{\mathcal{R}\epsilon}{2} = R_D$; thus when $\epsilon = \frac{2R_D}{\mathcal{R}}$, about half the reflected beam's area will overlap the detector's area.

XII. METHODS OF TESTING THE LENS

The collection efficiency $\mathcal{E}(\epsilon)$ curves calculated above assume the reflecting crystals are mounted tangentially to a true paraboloid. To decide how accurately the crystals must be aligned with this imaginary paraboloid, we observe that $\epsilon_{1/2} \approx .5°$ and that an error of .25° in θ causes as much defocusing as $\epsilon = .50°$. Thus to ensure a collection efficiency greater than 50% when $\epsilon = 0$, the errors in θ must be less than .25°. Accordingly I designed an optical device (see Fig. 23) which tests the actual "attitude" (i.e. the roll and pitch angles) of a salt crystal lying on the Silkspan skin which covers the lens frame. The second mirror's support can be slid to any position along the aluminum arm which, in turn can be rotated through 360°. Thus, the second mirror functions as a lightweight, moveable source of light propagating parallel to the axis of the x-ray lens. Clearly, the measured value of θ (the crystal's "pitch" or inclination angle) is

$$\theta_{meas} = \frac{1}{2} \tan^{-1}\left(\frac{a}{b}\right), \tag{110}$$

where a is measured to the center of the illuminated spot on the screen. For the values of b used ($b \tilde{=} 27$ inches), a 1° change in θ produces approximately a 1 inch change in a. When the device is accurately aligned, measurements made with it are readable to $\pm \frac{1}{16}°$, repeatable to at least $\pm \frac{1}{8}°$, and accurate to $\pm \frac{1}{4}°$ absolutely (at least for radial settings of 18 inches and less). Measurements of the roll angle can be made just as accurately, but a

rotation of the reflecting planes about their normal changes neither the direction of the reflected ray nor the reflecting power of a crystal. Thus the roll angle need not be measured.

The pitch angles of the crystals can be checked with an x-ray machine if one builds a mounting device capable of holding a detector at the lens' focal point while a well-collimated beam of x-rays is directed (parallel with the telescope's axis) at the part of the lens to be tested and the counting rate is monitored. The detector should be small enough (less than 1 inch in diameter for this lens) to detect significant defocusing, and the incident x-ray beam should be broad enough in area (more than .007 cm^2) and energy bandwidth (a few KeV) to insure that the number of photons reflected per second is just

$$N'(E) = \frac{dN}{dE} E \frac{R}{\theta_B} \qquad (111)$$

(from equations 18 and 54) where R is the "theoretical" optimum reflecting power (calculated assuming g = 260). If the actual counting rate is less than the rate predicted by equation 111, the reflecting crystal may be oriented improperly or may have the wrong thickness. Such tests with an x-ray machine give no information about crystal orientation that cannot be determined optically (with relative ease and precision), so this type of tester has not been built.

It is also possible to use the x-ray lens to focus x-rays from a point source a finite distance away. Figure 24 shows the geometry of this focusing. X-rays of energy E are emitted by a

source at point Q and reflected at point P (a radial distance $\bar{y}$ from the telescope's axis) to point O' provided that the "glancing angle" θ' satisfies the Bragg condition for nth order reflections; that is, reflection can occur if

$$\theta' \tilde{=} \theta_B\ (n,E) \tag{112}$$

where n may have to be chosen larger than 1 since we must have

$$\theta' > \theta\ . \tag{113}$$

The angle θ between the normal vector $\hat{n}$ at P and the telescope's axis is given by

$$\theta(\bar{y}) = \frac{1}{2}\tan^{-1}\frac{2y\mathcal{R}}{\mathcal{R}^2-y^2} \tag{114}$$

(from equations 6 and 7), where $\frac{\mathcal{R}}{2}$ is the lens' focal length, f. Using these values of θ' and θ we can determine where to put the source and the detector from the following formulas:

$$S \equiv QU = \frac{\bar{y}}{\tan(\theta'-\theta)} \tag{115}$$

$$S' \equiv UO' = \frac{\bar{y}}{\tan(\theta'+\theta)} \tag{116}$$

$$s \equiv QT = S - \Delta z = \frac{\bar{y}}{\tan(\theta'-\theta)} - \frac{\bar{y}^2}{2\mathcal{R}} \tag{117}$$

$$s' \equiv TO' = S' + \Delta z = \frac{\bar{y}}{\tan(\theta'+\theta)} + \frac{\bar{y}^2}{2\mathcal{R}}. \tag{118}$$

To calculate the expected counting rate c' of a detector at O' when a source of activity A_o disintegrations per second (1 curie = 3.7×10^{10} sec^{-1}) is located at Q we proceed as in section X, noting, however, that the glancing angle for the ith crystal is now θ_i' and the crystal's thickness, T_i, is no longer the optimum

thickness for the energy of the focused x-rays. The incident intensity I_o at P will be

$$I_o = \frac{A_o}{4\pi(S^2 + \bar{y}^2)} \tag{119}$$

and the new effective area becomes

$$A'_{lens}(E) = \frac{c'}{I_o} = A_c\, S'(E) \tag{120}$$

where

$$S'(E) = \sum_{i=1}^{N} \rho_i\,(\theta_i', E, T_i, n)\,\cos\theta_i'. \tag{121}$$

Provided that θ' is not much greater than θ, $S'(E)$ will be nearly as smooth as $S(E)$, so we can write

$$S'(E) \equiv \frac{1}{\Delta E} \int_{E-\frac{\Delta E}{2}}^{E+\frac{\Delta E}{2}} \sum_{n=1}^{N} \rho_i(\theta_i', E, T_i, n)\,\cos\theta_i'\, dE \tag{122}$$

$$= \frac{1}{\Delta E}\,\Delta N \cos\theta_B\, E.B.\,(E, \bar{T}, n) \tag{123}$$

where $\bar{T}$ is the average thickness of the ΔN crystals which are in a position to reflect photons of energy in the range $E \pm \frac{\Delta E}{2}$. Thus

$$A'_{lens}(E) = \frac{dA}{dE}\,\cos\theta_B\, E.B.\,(E, \bar{T}, n) \tag{124}$$

where now

$$\frac{dA}{dE} = \frac{dA}{d\theta}\,\frac{d\theta}{d\theta'}\,\left|\frac{d\theta_B}{dE}\right| \tag{125}$$

since the glancing angle is now θ', not θ. To a good approximation (for small θ'),

$$\theta = \theta' - \frac{Y}{S} \tag{126}$$

and

(127) $$y = \mathcal{R}\theta$$

so that we obtain

(128) $$\theta = \theta' \frac{S}{S + \mathcal{R}}$$

and

(129) $$\frac{d\theta}{d\theta'} = \frac{S}{S + \mathcal{R}} .$$

Thus the effective area for finite S becomes

(130) $$A'_{lens}(E) = \frac{\pi \mathcal{R}^2 S}{S + \mathcal{R}} R(E, \bar{T}, n) \sin 2\theta_B .$$

It can be shown from equation 48 that

(131) $$R(E, \bar{T}, n) = R(E, T_{o_{opt}}, n) \frac{\bar{T}}{T_{o_{opt}}} e^{1 - \bar{T}/T_{o_{opt}}} .$$

Thus, if the same order reflection is used in the finite S and infinite S geometries, we can express $A'_{lens}(E)$ in terms of $A_{lens}(E)$ (eq. 85) as

(132) $$A'_{lens}(E) = A_{lens}(E) \frac{S}{S + \mathcal{R}} \frac{\bar{T}}{T_{o_{opt}}} e^{1 - \bar{T}/T_{o_{opt}}},$$

which is always less than $A_{lens}(E)$.

The actual counting rate is then compared with c' (calculated from eq. 120):

(133) $$c' = \frac{A_o}{4\pi(S^2 + \bar{y}^2)} A'_{lens}(E) .$$

Although as yet untried, this method of testing annular sections of the x-ray lens should be accurate and relatively easy, experimentally.

XIII. COMPARISON OF THE FOCUSING X-RAY TELESCOPE WITH OTHER X-RAY DETECTORS

Two possible versions of this focusing x-ray telescope are compared with other x-rays detectors in Table II and Fig. 25, which shows the minimum intensity detectable in 100 seconds (with 3σ confidence) assuming anticoincidence (shielding) efficiencies calculated by Webber (1967). All the detectors use sodium iodide crystals situated in some sort of shield.

Table II

Detector	Na I area cm^2	Anticoincidence Scintillator	Focusing	Opening Half Angle	Reference
Peterson A	9.4	Cs I	No	$\sim 10°$	Peterson et al., 1965
Peterson B	40	Cs I (Na)	No	3°	Peterson, 1966
Reinert	100	Liquid	No	$\sim 10°$	Webber, 1967
Lindquist A	20	Plastic	6'dia. lens	0.5°	
Lindquist B	20	Cs I	6'dia. lens	0.5°	

Although liquid and plastic scintillators are efficient detectors of charged particles, their low atomic numbers makes their cross sections for x-ray absorption quite low. Thus, when used as guard detectors for an x-ray telescope, they are supplemented by passive shielding (e.g. lead and tin).

Both versions of this focusing telescope (which differ only in

the type of anticoincidence which is used) have considerably greater sensitivity at 30 KeV than the other detectors listed, but the advantage diminishes rapidly with increasing energy. The focusing telescope has by far the narrowest field of view of the detectors listed.

XIV. APPLICATIONS OF THIS FOCUSING X-RAY TELESCOPE

This focusing telescope's good sensitivity (especially in the 20-40 KeV energy range, where the flux detected at balloon altitudes is greatest) make it well suited for collecting data on weak sources in short times or discovering new sources, provided that it can be kept pointed accurately at the region of interest. If the telescope is made to scan across a several-square-degree area of the sky, strong sources can be located to a precision better than one degree as long as the instantaneous direction of the telescope's axis is known (though not necessarily controlled) to that accuracy. Anisotropies in the "isotropic" flux of extraterrestrial x-rays might also be detected.

XV. PROBLEMS ASSOCIATED WITH THE FOCUSING X-RAY TELESCOPE

Because the x-ray reflecting power of crystals is so small, the lens diameter must be much greater than the detector diameter if appreciable gain is to be realized. For a given energy range, the range of Bragg angles is fixed, so the effective area of the lens can only be increased by making the lens larger and putting it farther away from the detector, thereby decreasing the field of view (since the detector then subtends a smaller angle as seen from the lens). In the case of this telescope, the finite size of the crystals, crystal mounting irregularities, and the appreciable width of the curve $\rho(\theta)$ for rock salt can contribute to defocusing nearly as large as the nominal opening half angle: 0.5°. So increased gain with this type of telescope seems impossible.

Moreover, an opening half angle of 0.5° or less requires considerable precision in the machining of the pieces for the lens frame. Because of variations of about .010" in hole locations on the spokes of the original lens frame, this frame had to be scrapped. In its place, an all-aluminum 3 ft. diameter lens frame with a local length of 57.3 in. is being built.

Devices capable of accurately determining the celestial coordinates toward which the telescope is pointed must also be developed. I presently plan on using a two-dimensional

sun sensor and a gravity sensor (whose outputs will be telemetered, along with detector rate and pulse height data) for pointing direction information. Control of the telescope's elevation and azimuth will be achieved by radio command.

XVI. POLARIZATION MEASUREMENTS

In calculating the effective area of this lens, we replaced $\sin^2\phi$ in equation 23 by its average value (averaged over all possible polarization directions),

$$\overline{\sin^2 \phi} = \frac{1 + \cos^2 2\theta}{2} . \tag{134}$$

This was permissible for this lens, since its symmetry (about the z-axis) implies that for a given x-ray the plane of incidence may be at any angle to the plane of polarization of the x-ray. The gain curve calculated above thus applies no matter how polarized the incident x-radiation may be.

With a slight modification, this focusing telescope can (in principle, at least) be used to detect and measure polarization of x-rays. For radiation with its electric field vector in the plane of incidence (the plane containing incident and reflected wave vectors),

$$\sin^2\phi = \cos^2 2\theta, \tag{135}$$

whereas for radiation with its electric field vector perpendicular to the plane of incidence,

$$\sin^2 \phi = 1. \tag{136}$$

Thus the reflecting powers of a crystal for the two cases of polarization are related by

$$R_{\parallel} = \cos^2 2\theta \; R_{\perp}. \tag{137}$$

Thus if the radiation falling on the lens is linearly polarized, the reflected intensity will be greatest from that part of the lens where the crystals' planes of incidence are approximately perpendicular to the plane of polarization. If a lead disk, with its center and two diametrically opposite sectors removed (see Fig. 26), is made to rotate underneath the lens, the counting rate will be greatest when the diameter between the removed sectors is perpendicular to the plane of polarization.

However, $R_{\parallel}$ and $R_{\perp}$ never differ by more than 9% for this lens, so the lens itself would have to be very uniform for this method to successfully detect even very strong polarization. And, unfortunately, the insertion of the rotating absorber reduces the counting rate (of x-rays from the source) by a factor of two or more (depending on how wide the sectors are), thereby reducing the telescope's sensitivity by that factor.

XVII. SOME POSSIBLE FUTURE DEVELOPMENTS

Other focusing x-ray telescopes might make use of nearly perfect crystals (e.g. calcite) which have large reflection coefficients over a very narrow range of glancing angle(or energy). Such telescopes could have great gain over a narrow energy interval, but would require great pointing control accuracy. And to take full advantage of this gain, the telescope's detector would have to have resolution about as fine as the bandwidth of the lens, so that background events of energy outside this bandwidth would not be confused with the signal.

Rocket-borne or satellite-borne x-ray telescopes might be designed for energies below 20 KeV. At energies below 30 KeV, the calculated reflecting power of rock salt (assuming $g = 260$) is approximately proportional to $E^{3/4}$, so R is smaller at lower energies. But, for a given focal length, the lens diameter will be proportional to $(\sin \theta_B)_{max}$, which, in turn, is inversely proportional to the minimum energy which will be focused. Thus one would expect a low energy telescope to have about the same gain as a higher energy telescope with the same opening angle. Since the incident intensity is, for a typical source of cosmic x-rays, much greater at these lower energies, the low energy telescope would be more likely to detect new sources, assuming our calculations are correct.

However, our calculations of R did not take into account primary extinction, which becomes important for rock salt at energies below about 20 KeV. Primary extinction occurs when the perfect blocks (of which a mosaic crystal is composed) are sufficiently large that appreciable extinction occurs in each of them. (Thus the probability of reflection by a block is no longer proportional to the block's volume.) This effect reduces the reflecting power of natural rock salt (in the Bragg case) to 4.0×10^{-4} at 17.2 KeV and 1.02×10^{-4} at 8 KeV (values measured by Compton (1917) and Renninger (1934), respectively). The effect can be largely eliminated by grinding the crystals (Renninger (1934) and Bragg (1921), but this method is not easily applied to the thin crystals used in the Laue case.

Focusing x-ray telescopes much better than the one I have designed could be constructed if crystals with much greater reflecting powers were available. The fundamental limitation on reflecting power is the ratio $\frac{Q}{\mu}$, which is just the ratio of integrated reflection probability to absorption probability for a small perfect crystal. If we consider, for simplicity, a crystal whose atoms are all the same, we can readily see the manner in which $\frac{Q}{\mu}$ varies with the density ρ of the crystal and the atomic number z of its atoms.

For small θ, the structure factor F approaches the number z_T of electrons in the unit cell of volume V:

$$F \tilde{=} z_T \ . \tag{138}$$

The electron density is $\frac{\rho}{A} z$, where A is the atomic weight of the crystal's atoms. Thus

(139) $$z_T = \frac{\rho}{A} z \quad V.$$

Since $\frac{z}{A}$ is fairly constant, equation 25 gives us

(140) $$Q \propto \left|\frac{F}{V}\right|^2 \approx \rho^2$$

where the symbol $\approx$ means "is roughly proportional to." For energies below 100 KeV

(141) $$\mu \propto z^4 \frac{\rho}{A}$$

(Bleuler and Goldsmith, 1960, p. 176).

Thus

(142) $$\frac{Q}{\mu} \approx \frac{\rho}{z^3} .$$

The density of a solid is a relatively slow function of its atomic number, so low -z crystals should have much higher reflecting powers than high -z crystals. The atomic numbers of the components of this lens are not very low (11 and 17 for sodium and chlorine, respectively), so there appears to be some hope of making a much more efficient x-ray lens by somehow fabricating ideally imperfect low -z crystals.

BIBLIOGRAPHY

Bleuler, Ernst and Goldsmith, George J., Experimental Nucleonics, New York, Holt, Rinehart and Winston, 1960.

Blokhin, M.A., X-Ray Spectroscopy, India (Delhi-6), Hindustan Publishing Corporation, 1962.

Bowyer, S., Byram, E.T., Chubb, T.A., and Friedman, H., Transactions, American Geophysical Union 45, 561, (1964).

Bragg, W.H., Philosophical Magazine 27, 881 (1914).

Bragg, W.L., James, R.W., and Bosanquet, C.H., Philosophical Magazine 41, 309 (1921).

Brini, D., Ciriegi, U., Fulgini, F., Gandolfi, A. and Moretti,E., Nuovo Cimento, XXXVIII, 130 (1965).

Compton, A.H., Physical Review 10, 95 (1917).

Friedman, H., announcement to the press, Minneapolis Star (July 7, 1967).

Giacconi, R., Gorenstein, P., Gursky, H., Usher, P.D., Waters, J.R., Sandage, A., Osmer, P. and Peach, J.V., Astrophysical Journal Letters to the Editor, 148, L 129 (June, 1967).

Handbook of Chemistry and Physics, Thirty-First Edition, Cleveland, Ohio, Chemical Rubber Publishing Co., 1949.

Haymes, R.C. and Craddock, W.L., Journal of Geophysical Research 71, 3261 (1966).

The Isotope Index 1963-1964, James L. Sommerville, editor, Indianapolis, Indiana, Scientific Equipment Co., 1963.

James, R.W., The Optical Principles of the Diffraction of X-Rays, London, G.Bell and Sons Ltd., 1948.

McCracken, K.G., paper read at the Washington meeting of the American Physical Society, April, 1967.

Ney, E.P. et al. (Balloon Project, Department of Physics, University of Minnesota), Buoyant Forces in the Standary Atmosphere (circular slide rule), 1964.

Peterson, L.E., Jacobson, A.S. and Pelling, R.M., University of California at San Diego preprint (UCSD-SP-65-5), December 21, 1965.

Peterson, L.E., proposal to the National Aeronautics and Space Administration (University of California, San Diego, UCSD 1929), October 5, 1966.

Renninger, M., Zeit. F. Krist. 89, 344 (1934).

Ulrey, C.T., Physical Review 11, 401 (1918).

Webber, W.R., private communication, 1967.

Zachariasen, W.H., Theory of X-Ray Diffraction in Crystals, New York, John Wiley and Sons, Inc., 1945.

Zachariasen, W.H., Physical Review Letters 18, 195 (1967). (Derivation to be published in Acta. Cryst.).

Zachariasen, W.H., private communication, 1967.

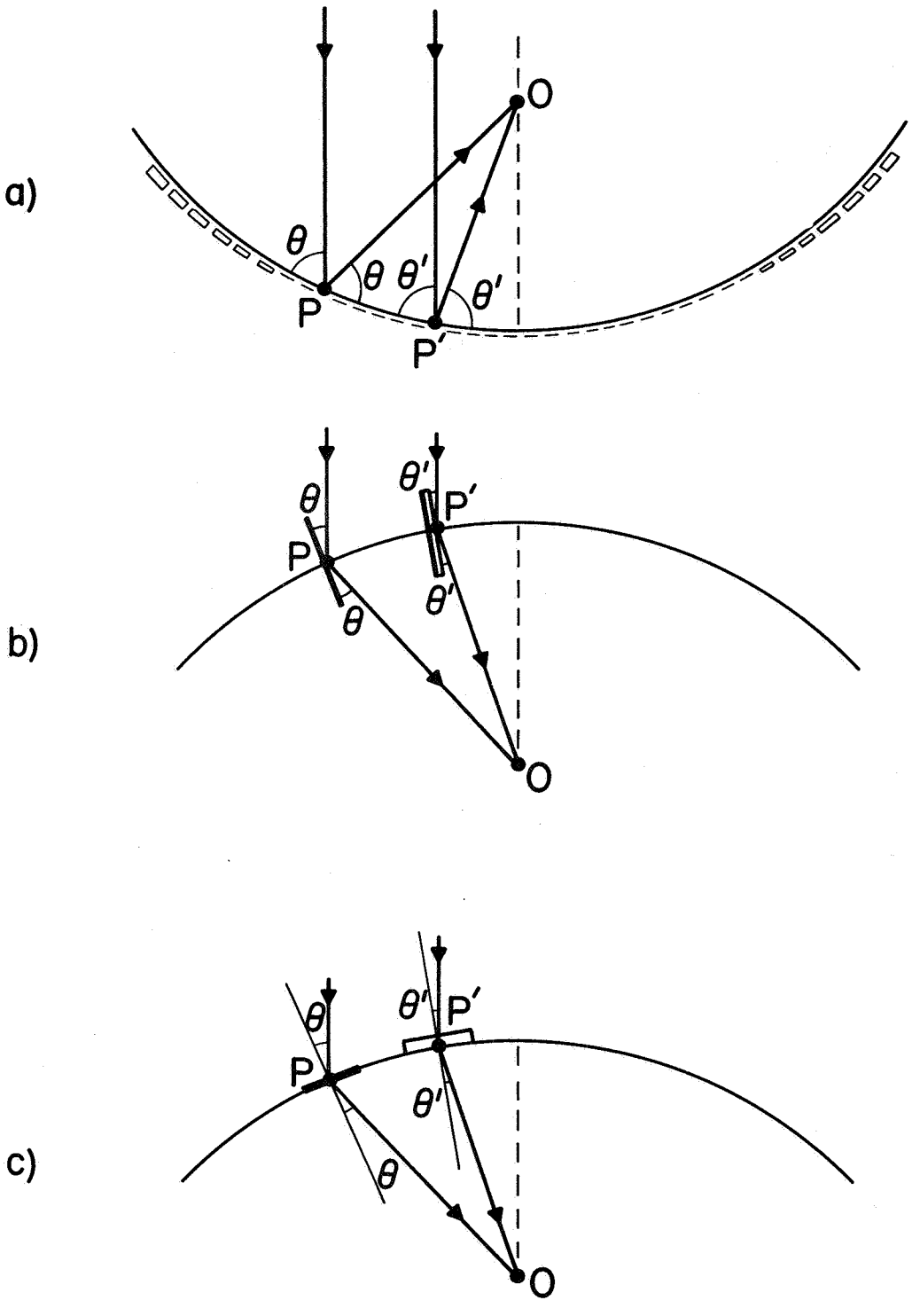

Figure 1. Three possible arrangements of crystals to form an x-ray lens.

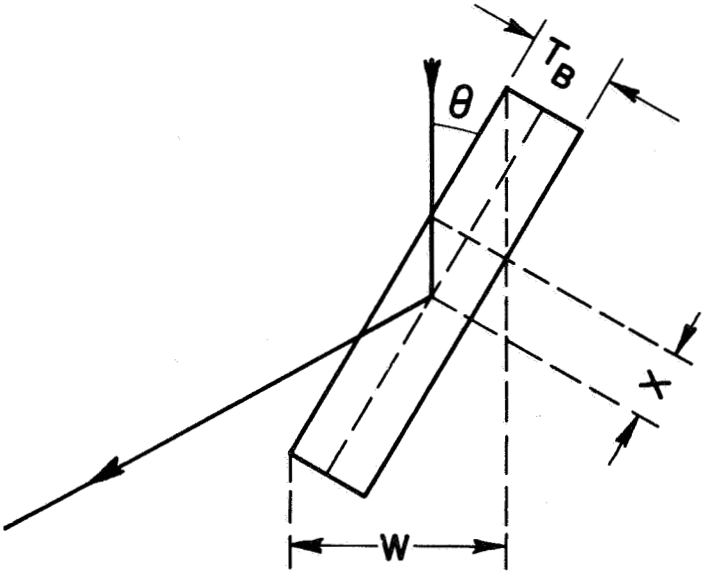

(a) BRAGG CASE

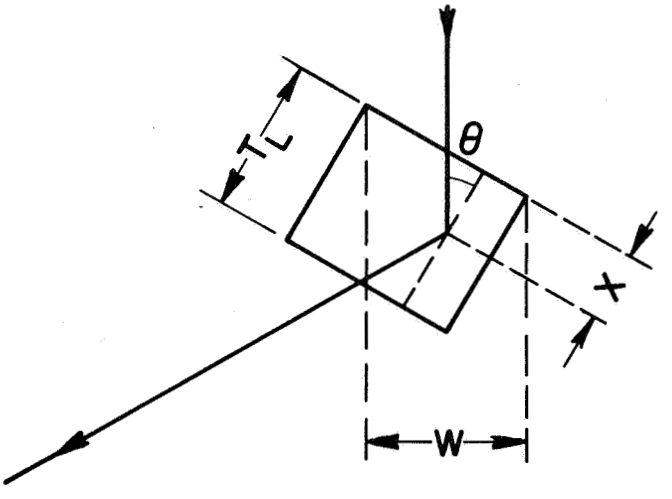

(b) LAUE CASE

Figure 2. The Braqq and Laue cases of x-ray reflection.

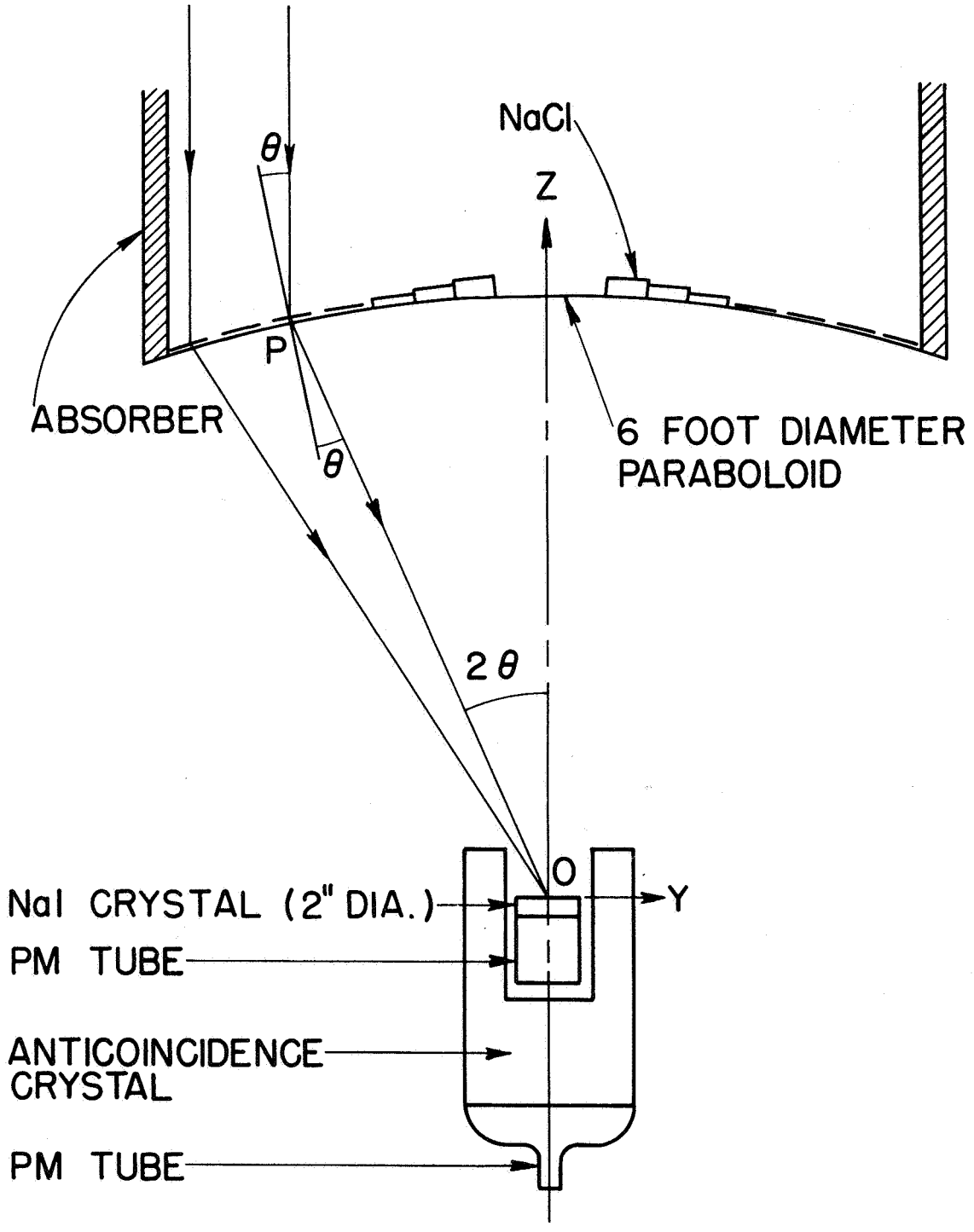

Figure 3. Schematic drawing of the focusing x-ray telescope (not to scale).

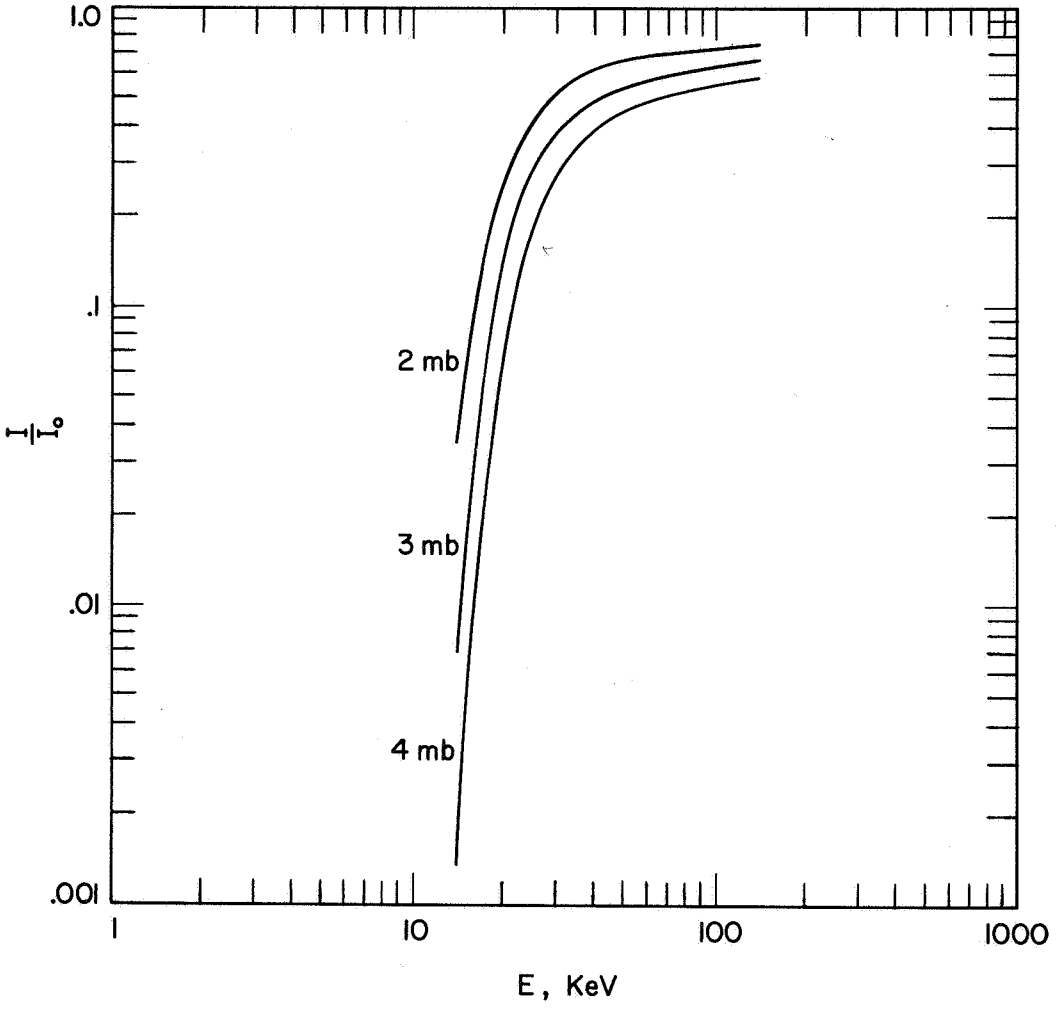

Figure 4. Atmospheric transmission of vertically incident x-rays at high altitudes (pressures in millibars).

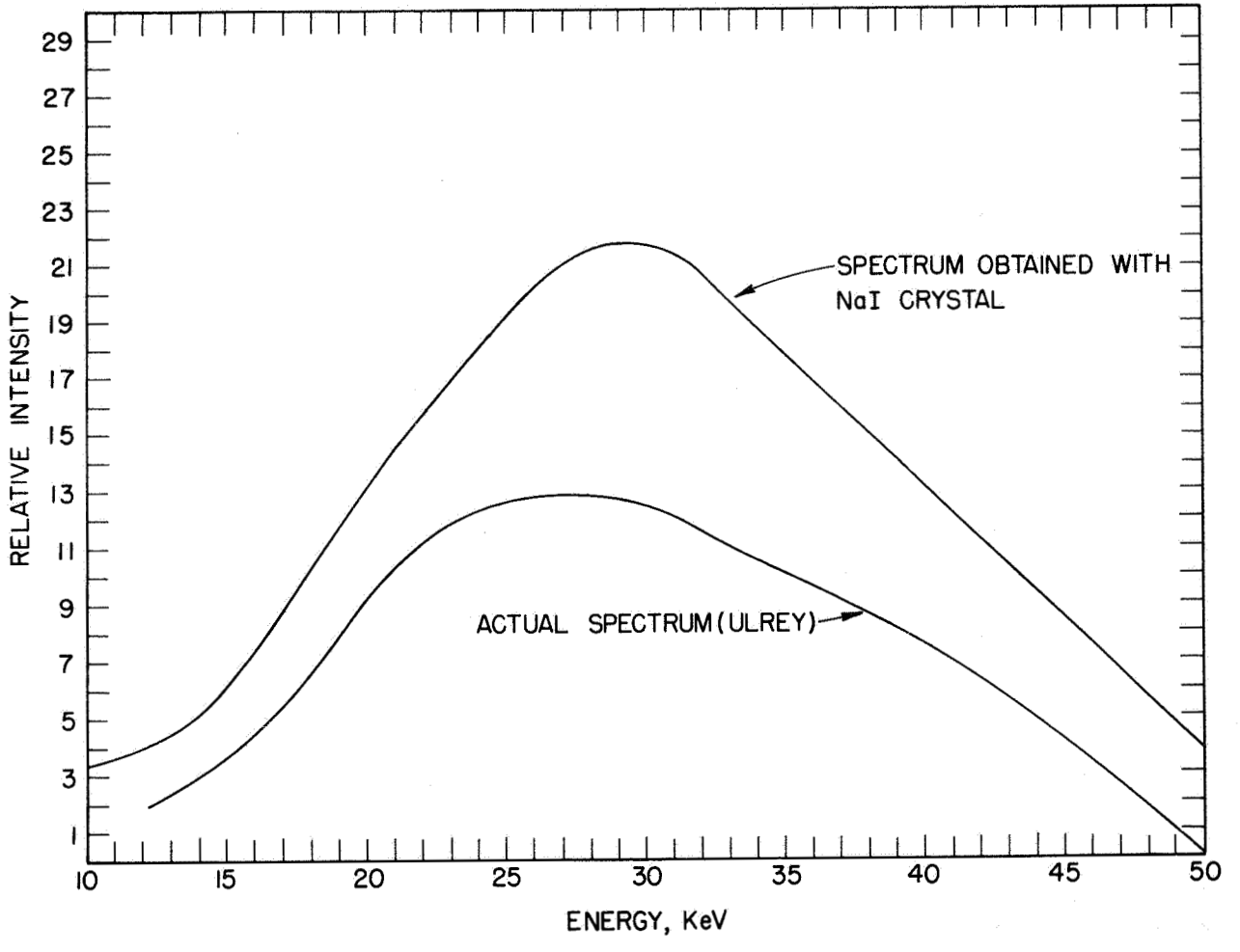

Figure 5. Spectra of x-rays from a tungsten target with an applied voltage of 50 kilovolts.

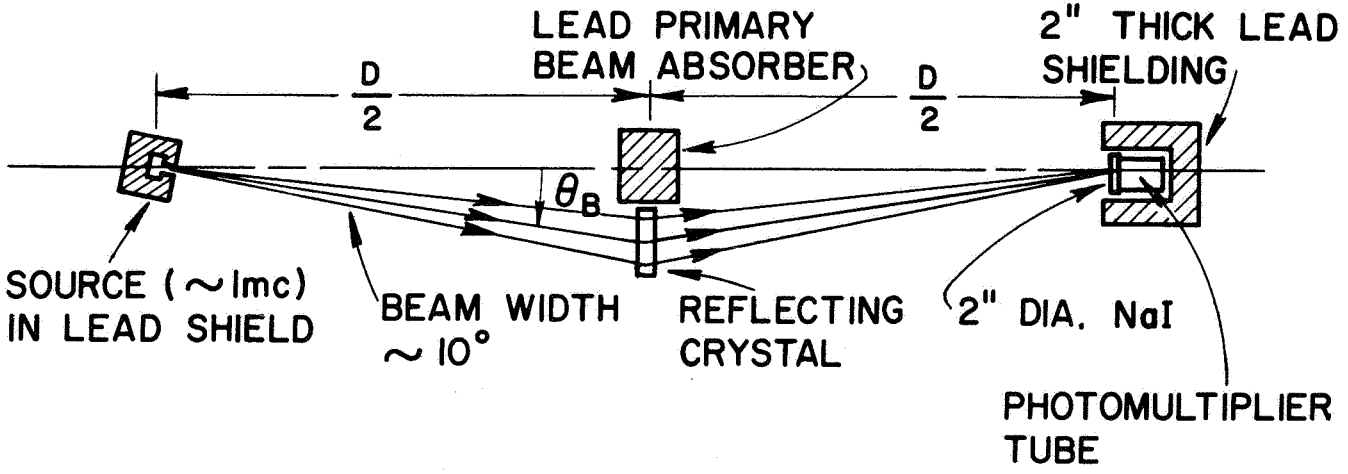

Figure 6. Geometry used in measuring reflecting power with x-rays from a radioactive source.

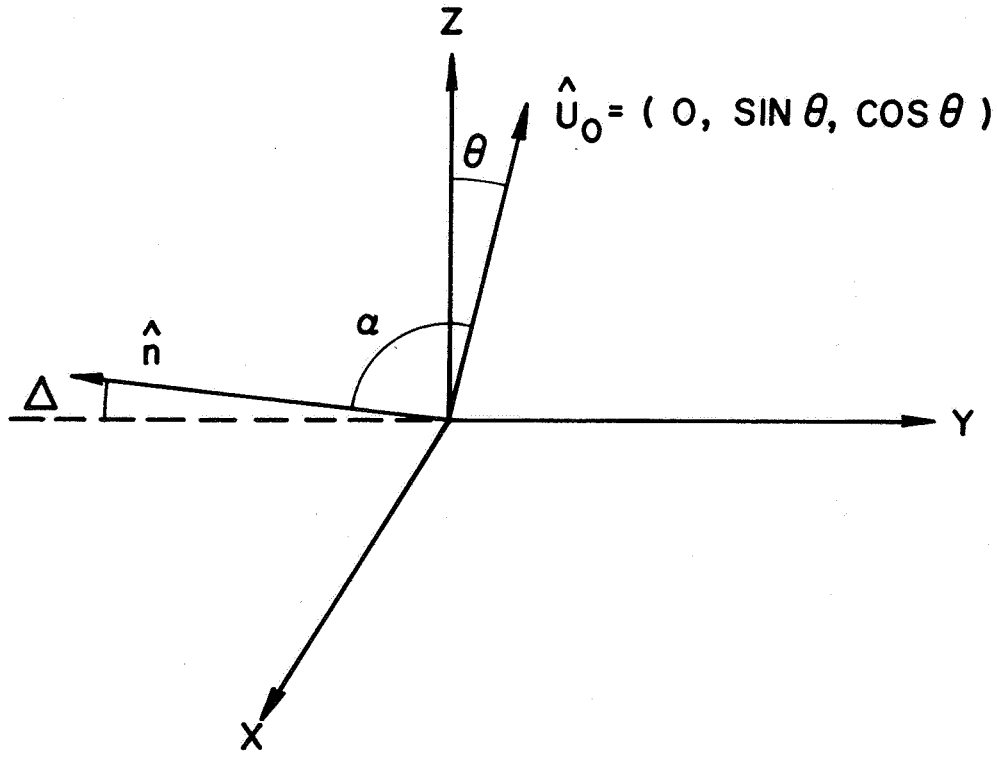

Figure 7. Unit vectors and angles occurring in the calculation of the reflecting power of a mosaic crystal.

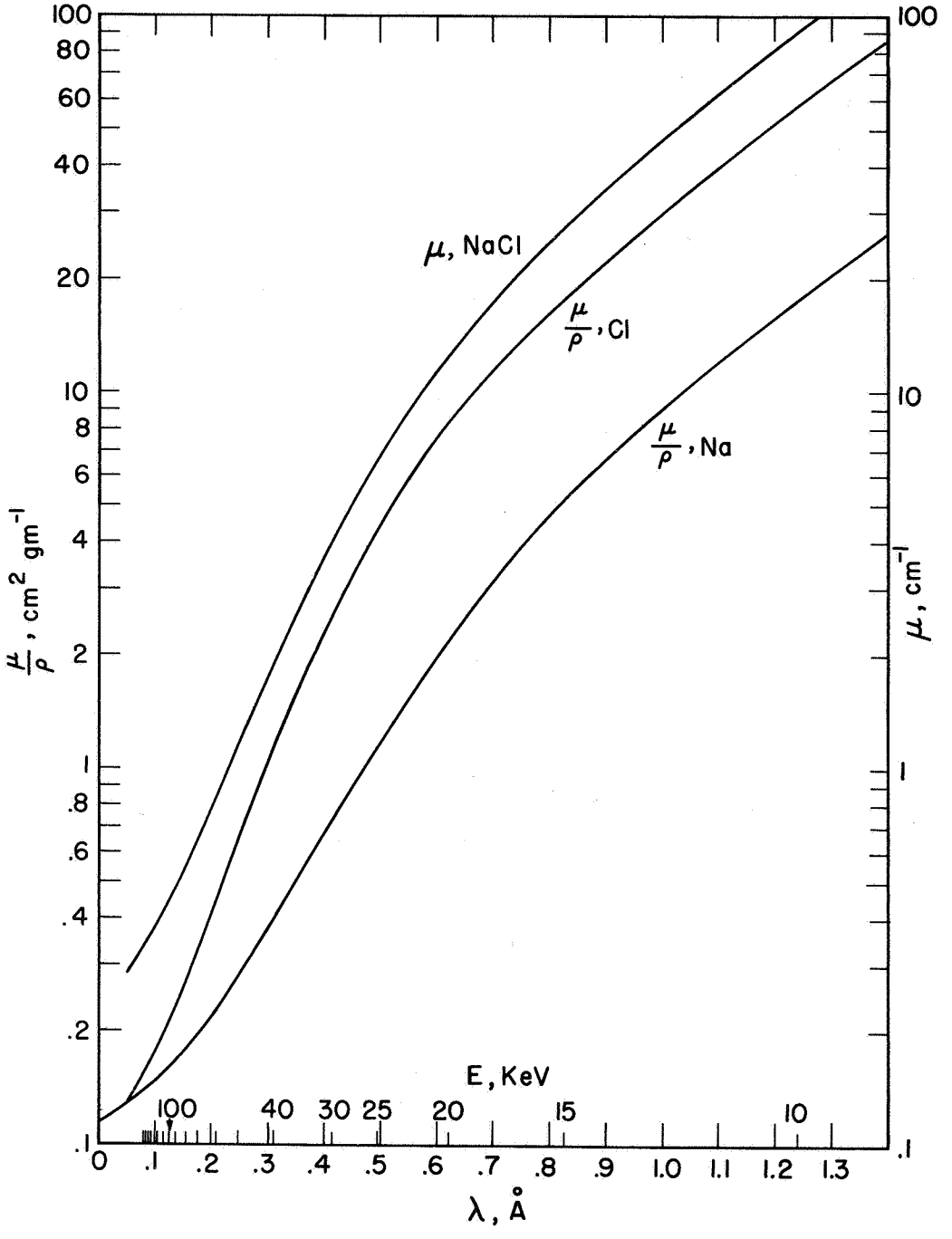

Figure 8. μ/ρ for Na, Cl and μ for NaCl as functions of x-ray wavelength or energy.

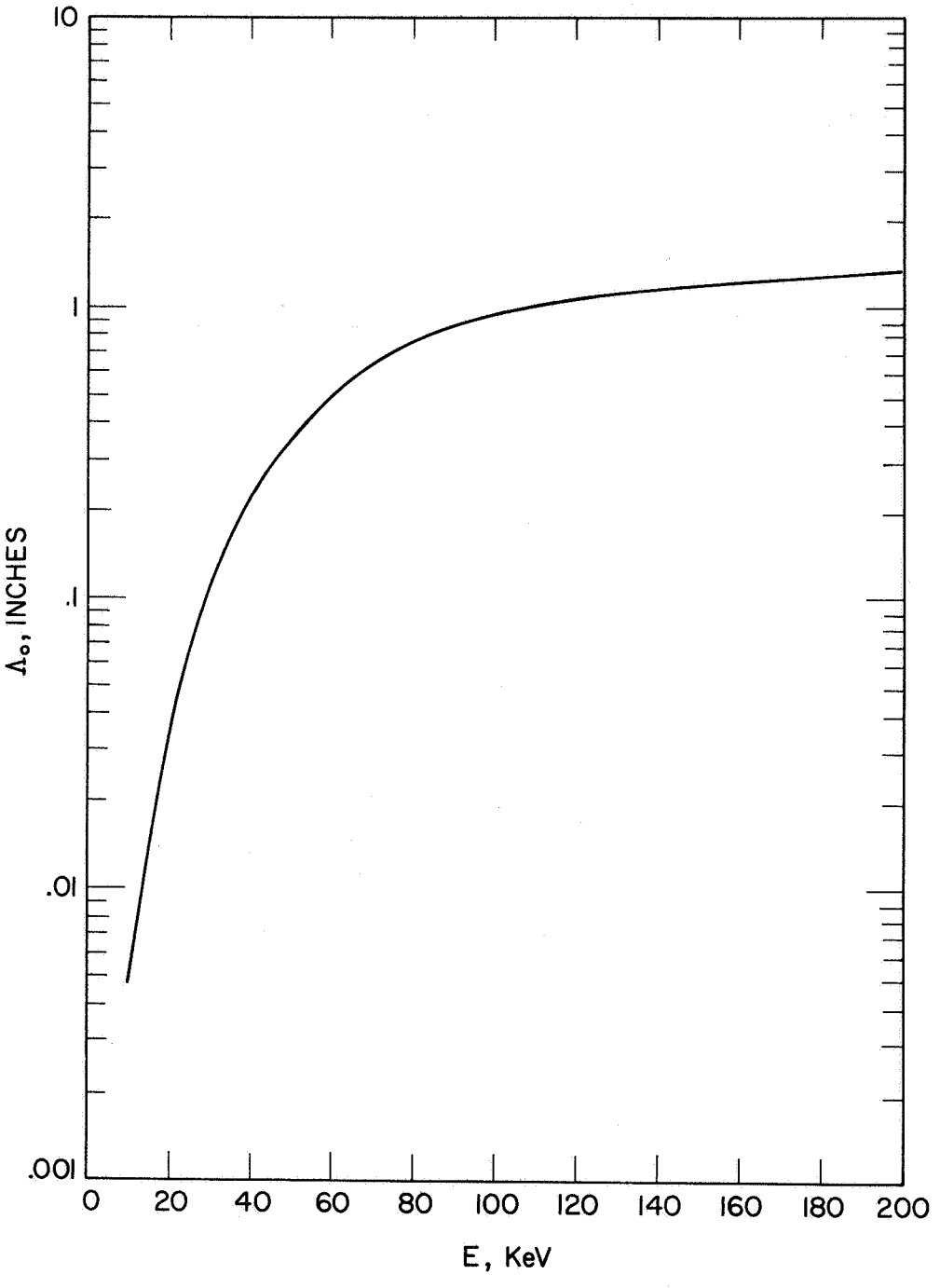

Figure 9. Absorption length for x-rays in rock salt as a function of energy.

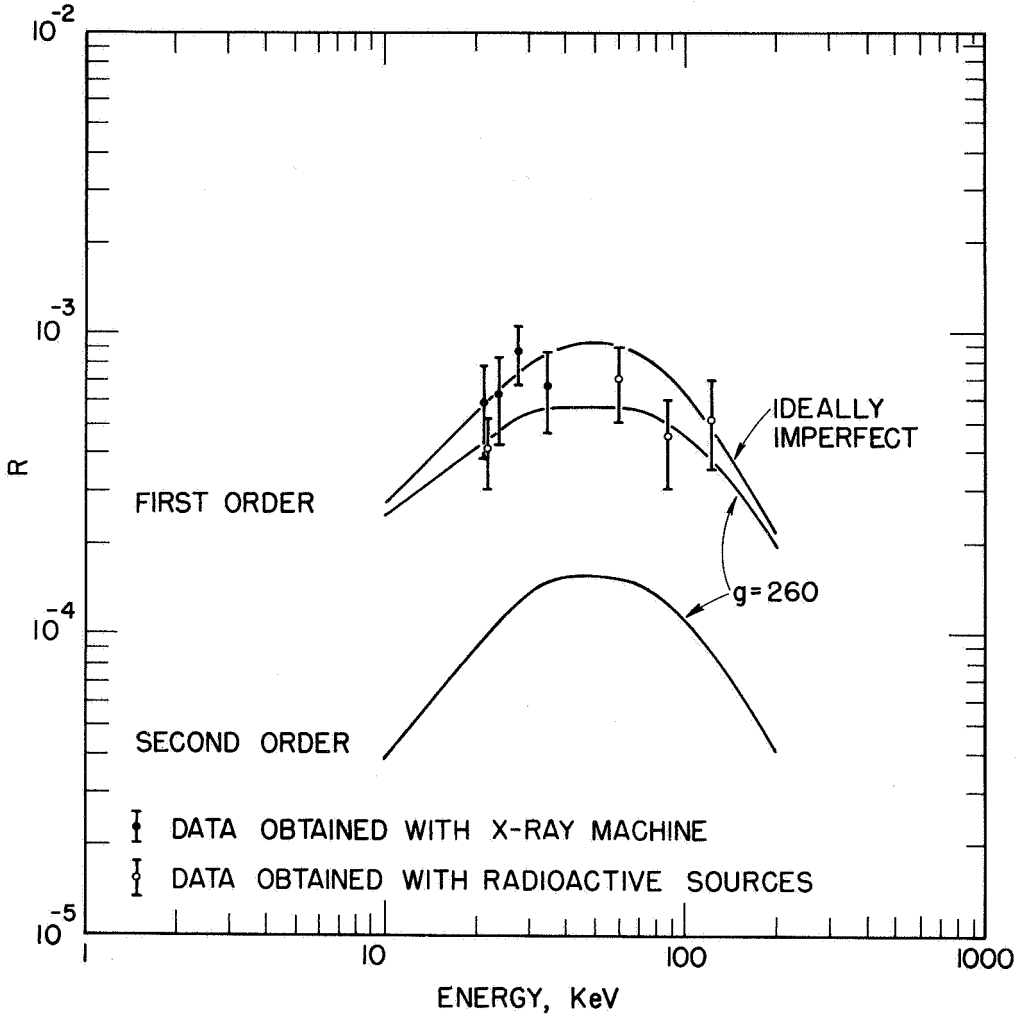

Figure 10. Reflecting power (Laue case) of rock salt crystals of optimum thickness.

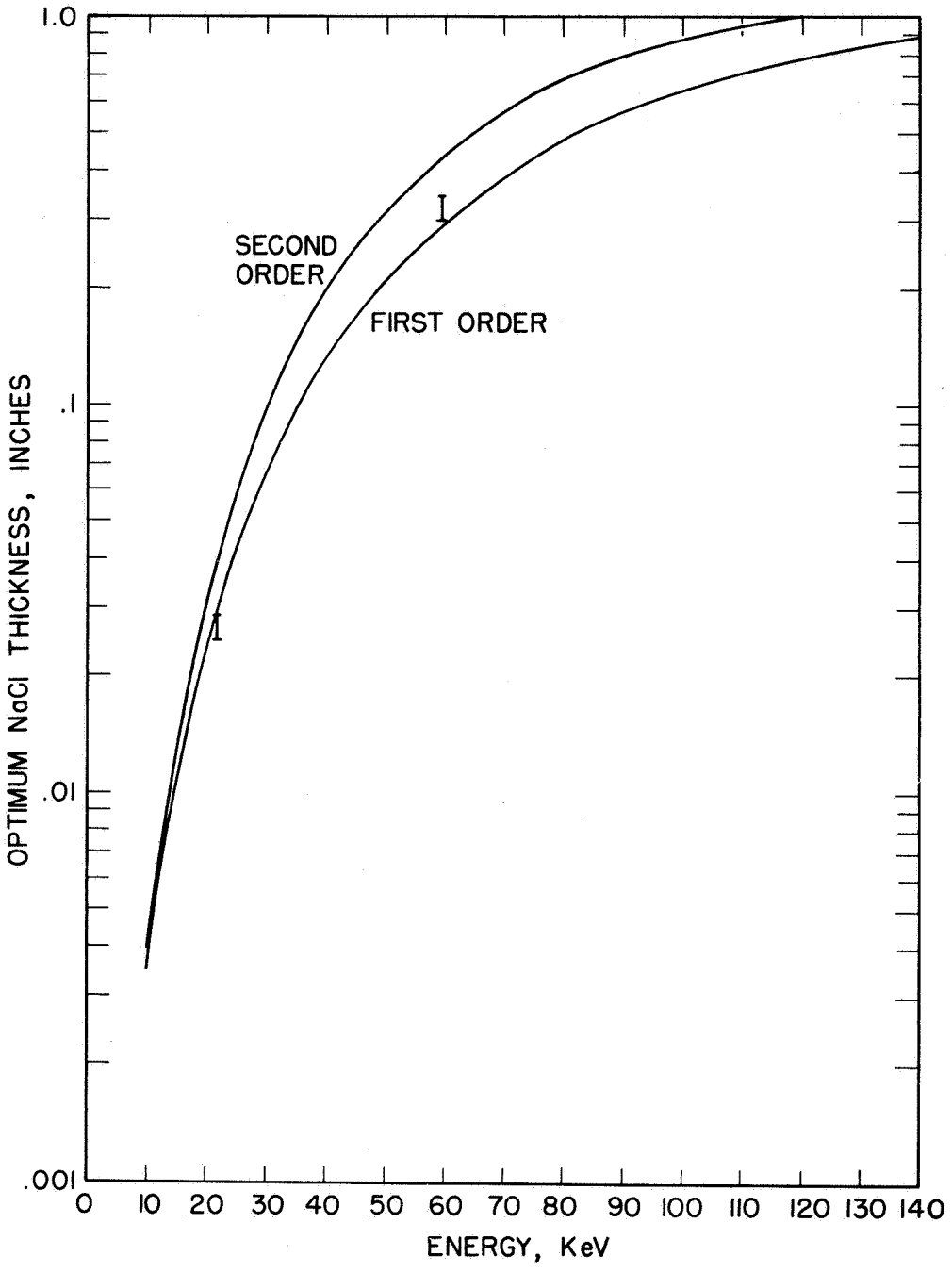

Figure 11. Optimum NaCl thickness as a function of energy.

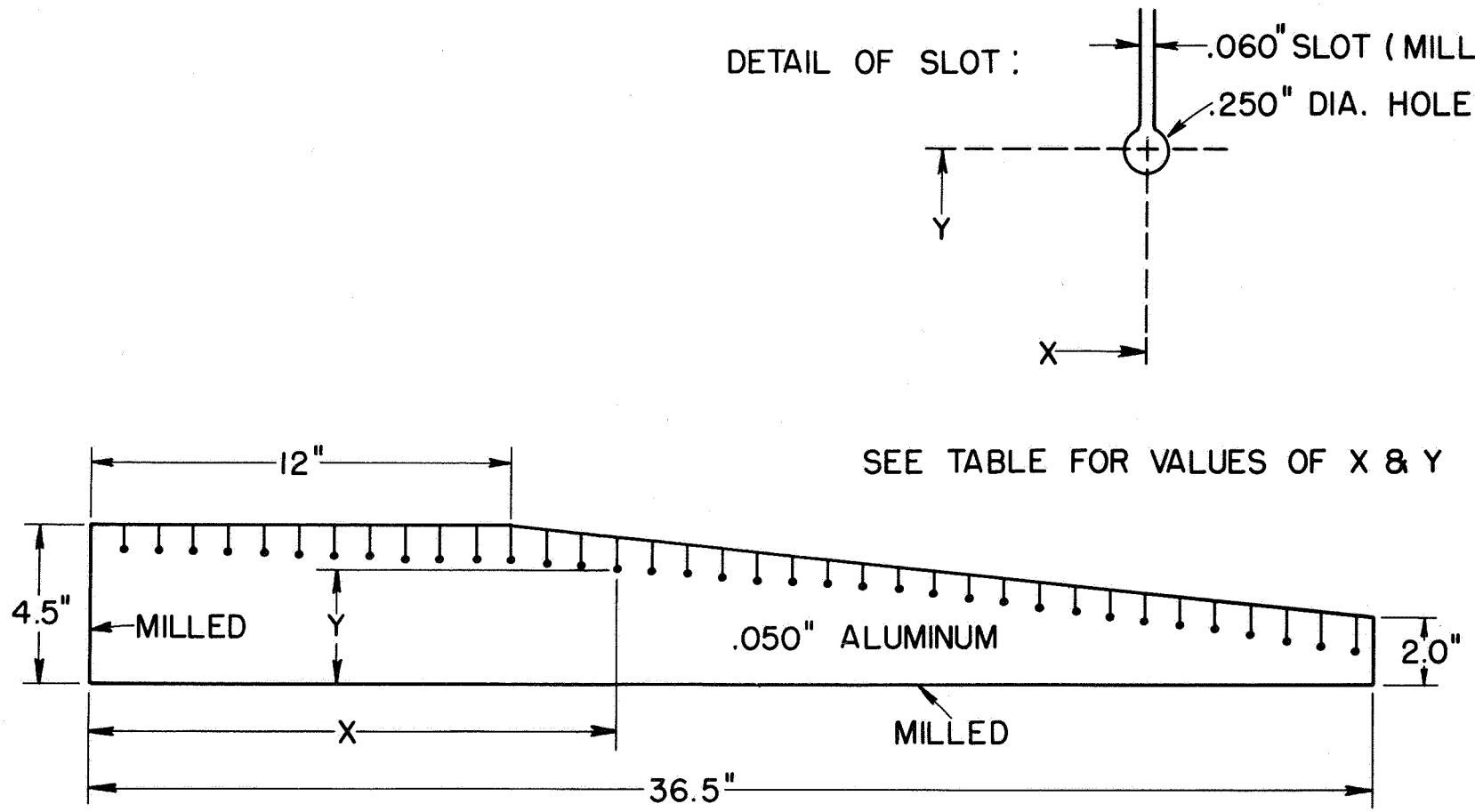

Figure 12. Spoke for parabolic frame.

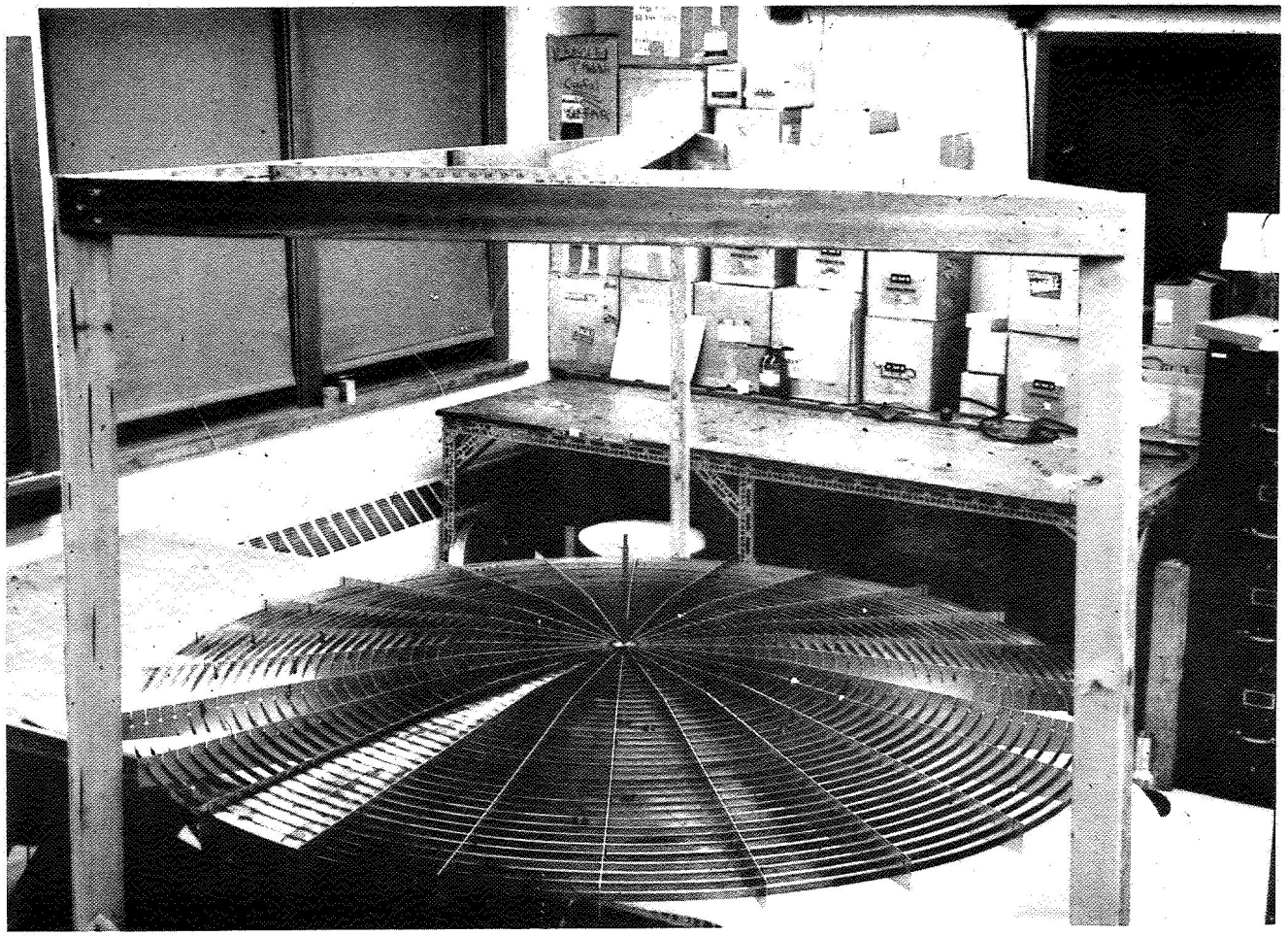

Figure 13. Parabolic frame for x-ray lens. The tripod surrounding the lens is a support for the optical testing device shown diagrammatically in Figure 23.

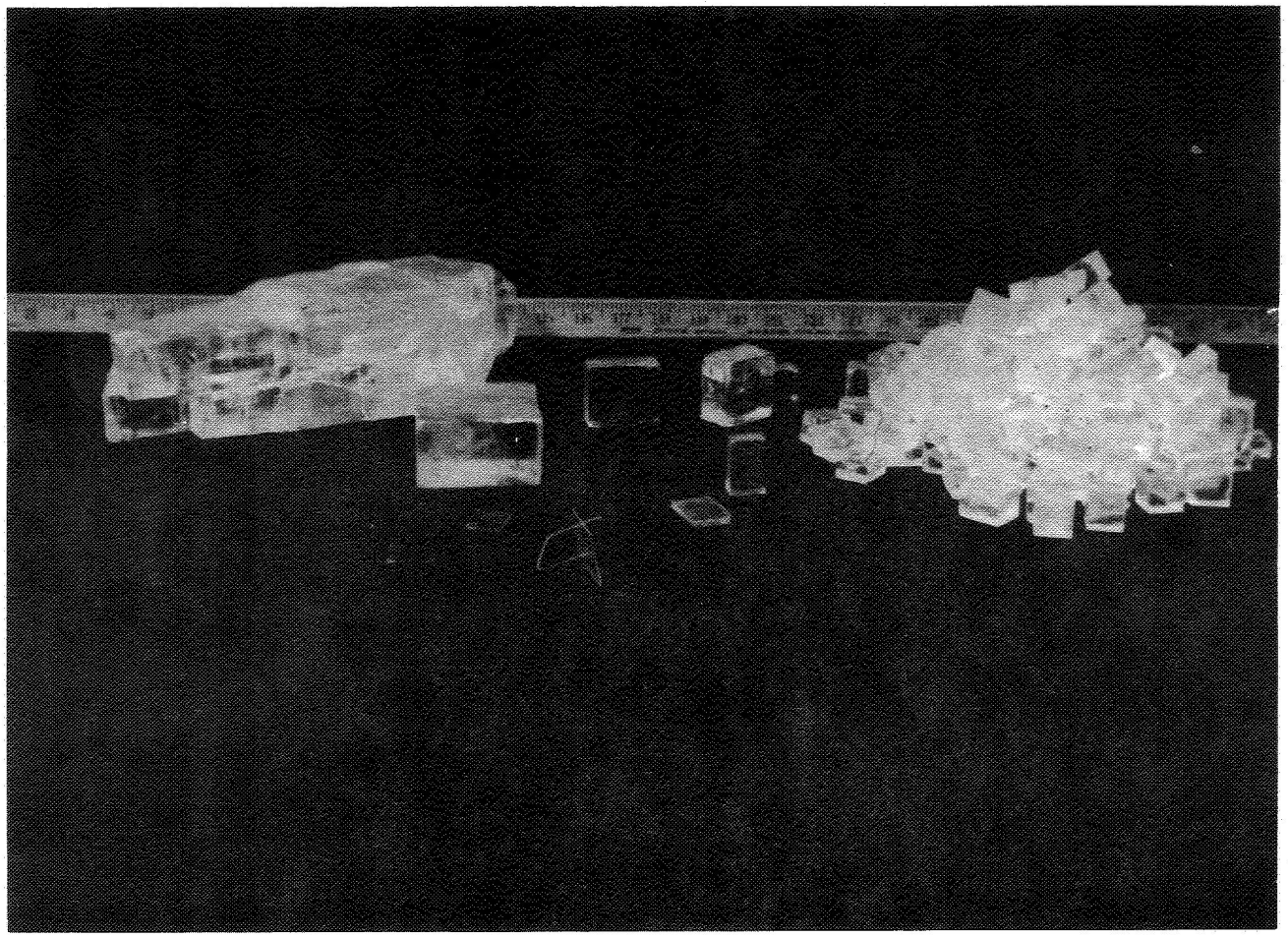

Figure 14. Rock salt, uncleaved and cleaved to various thicknesses.

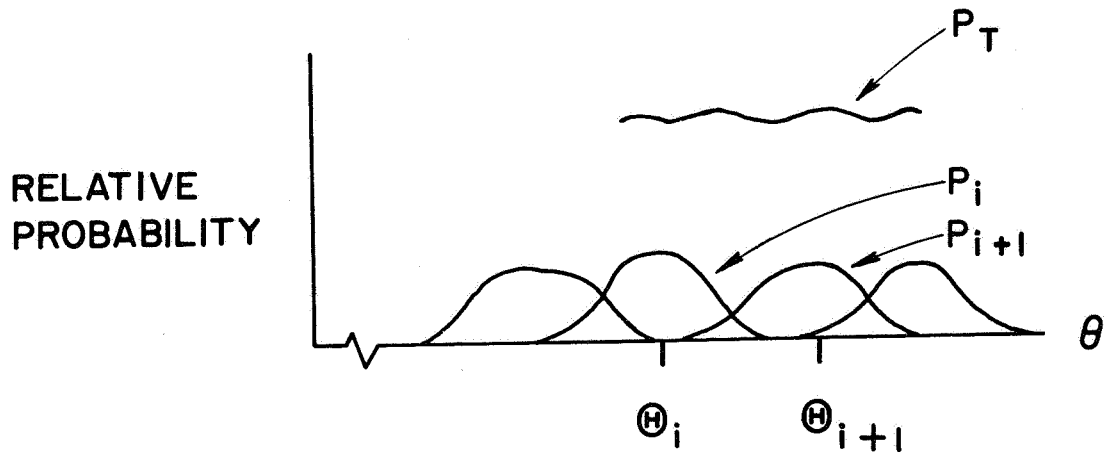

Figure 15. Summation of crystals' probability distributions in θ.

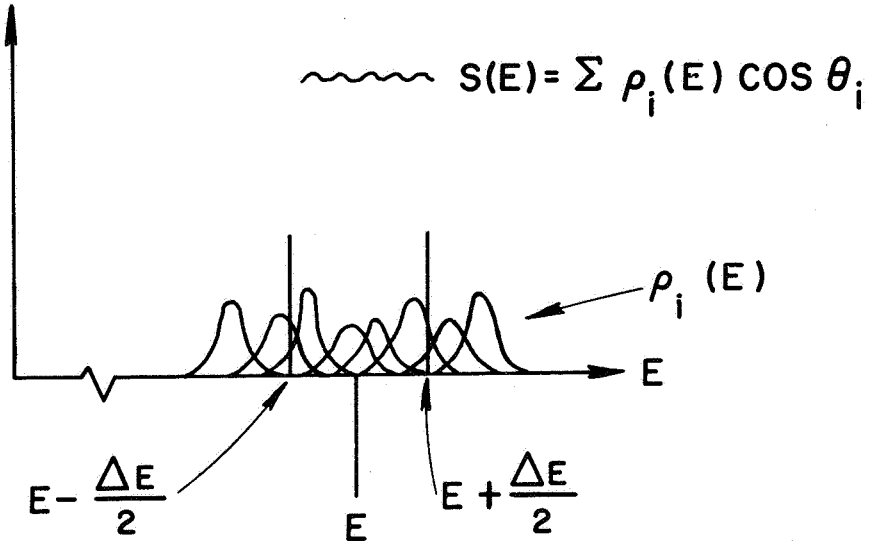

Figure 16. Summation of ρ_i's in the energy interval from $E - \frac{\Delta E}{2}$ to $E + \frac{\Delta E}{2}$.

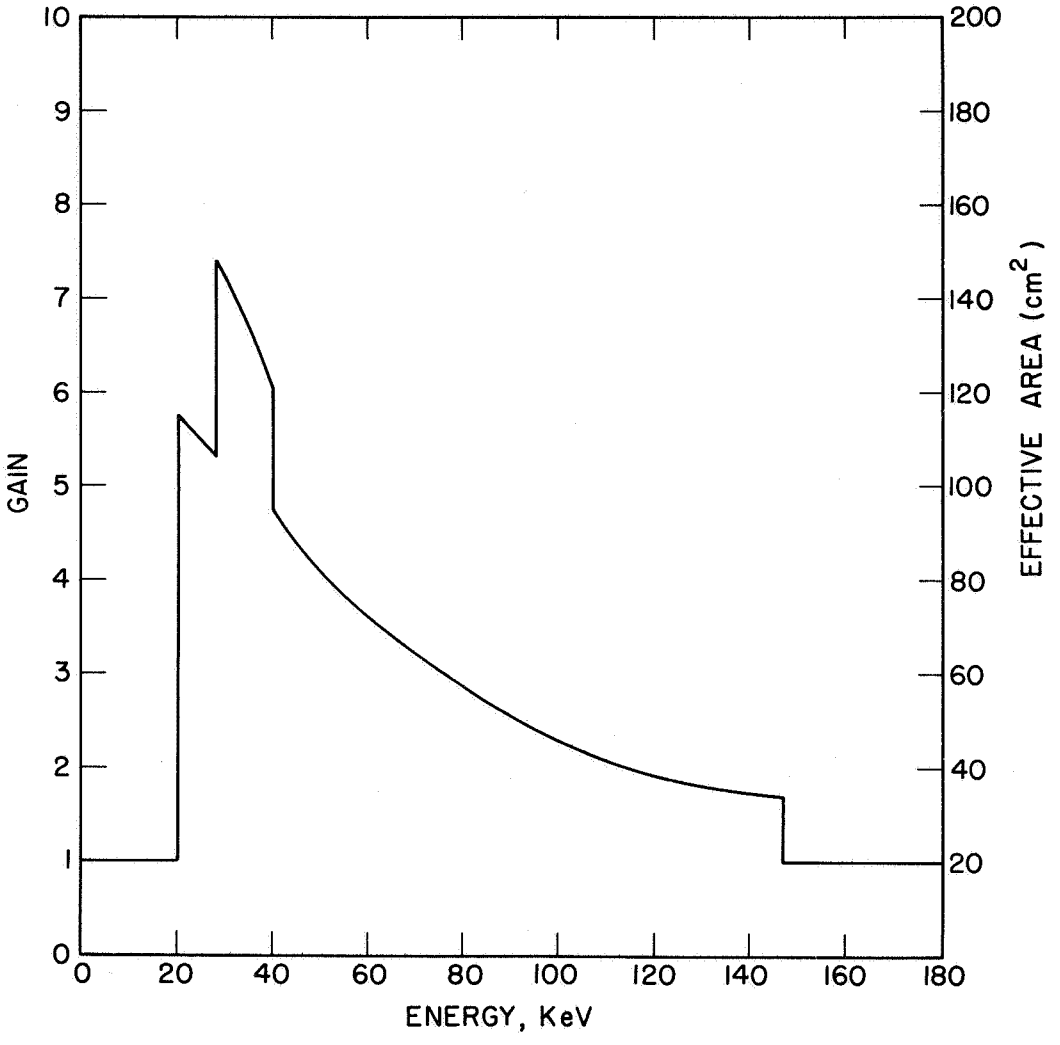

Figure 17. Effective area and gain of the focusing x-ray telescope.

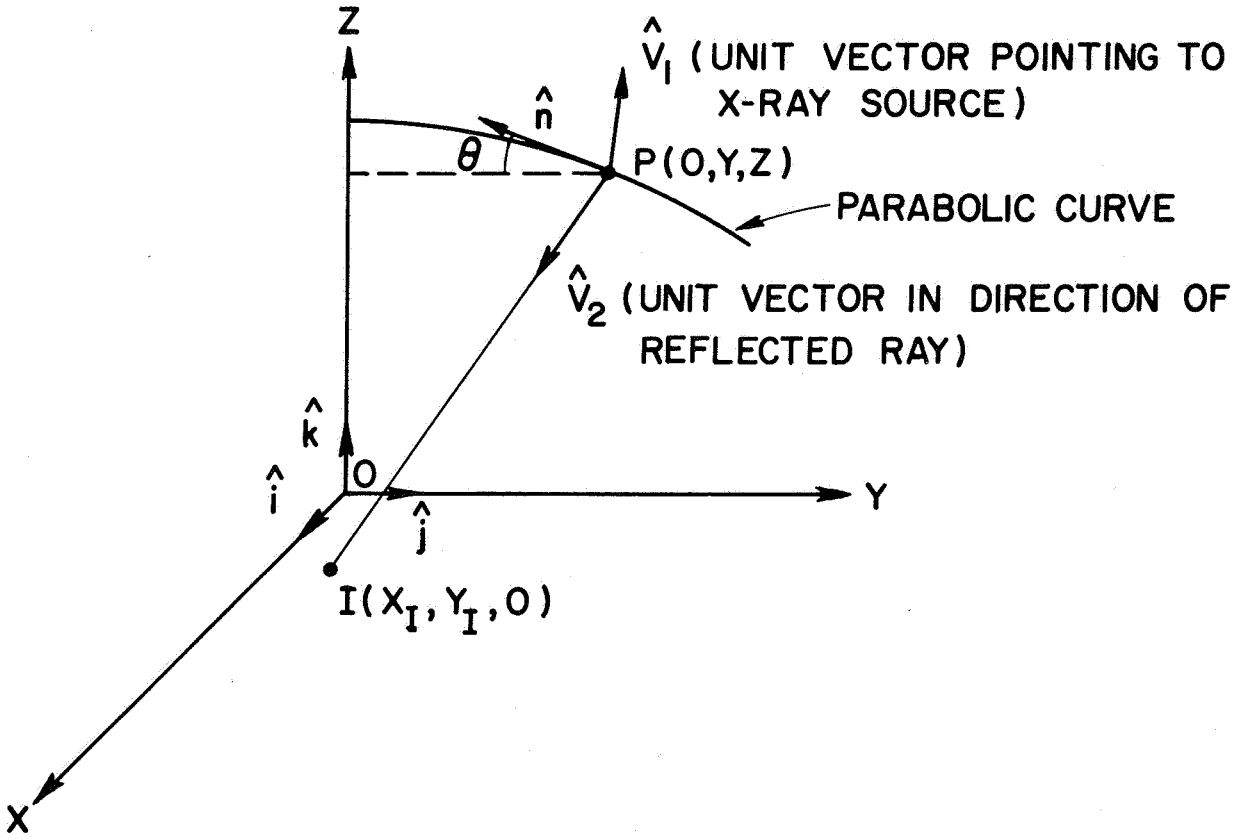

Figure 18. Geometry of x-ray reflection by a crystal of infinitesimal dimensions at P. The detector is in the x-y plane.

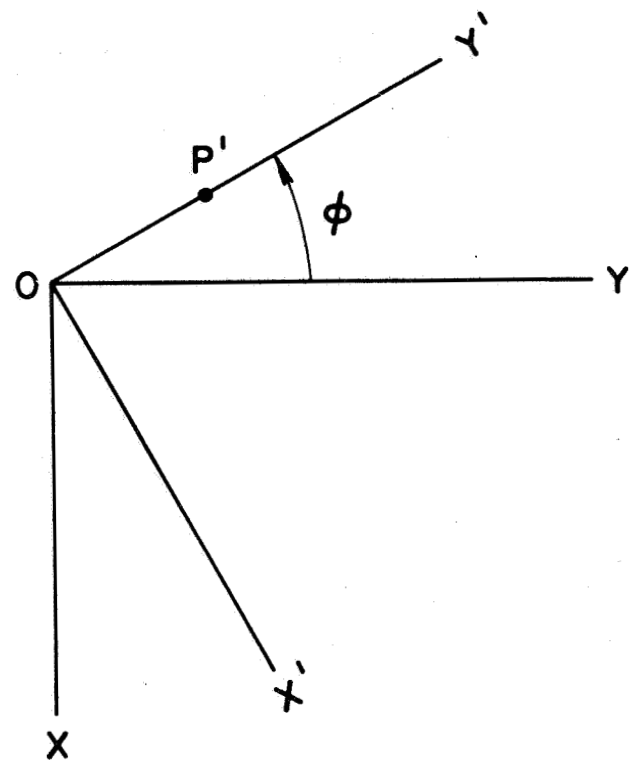

Figure 19. Top view of x, x', y and y' axes. Point P' lies on the paraboloid, whose focal point is the origin O.

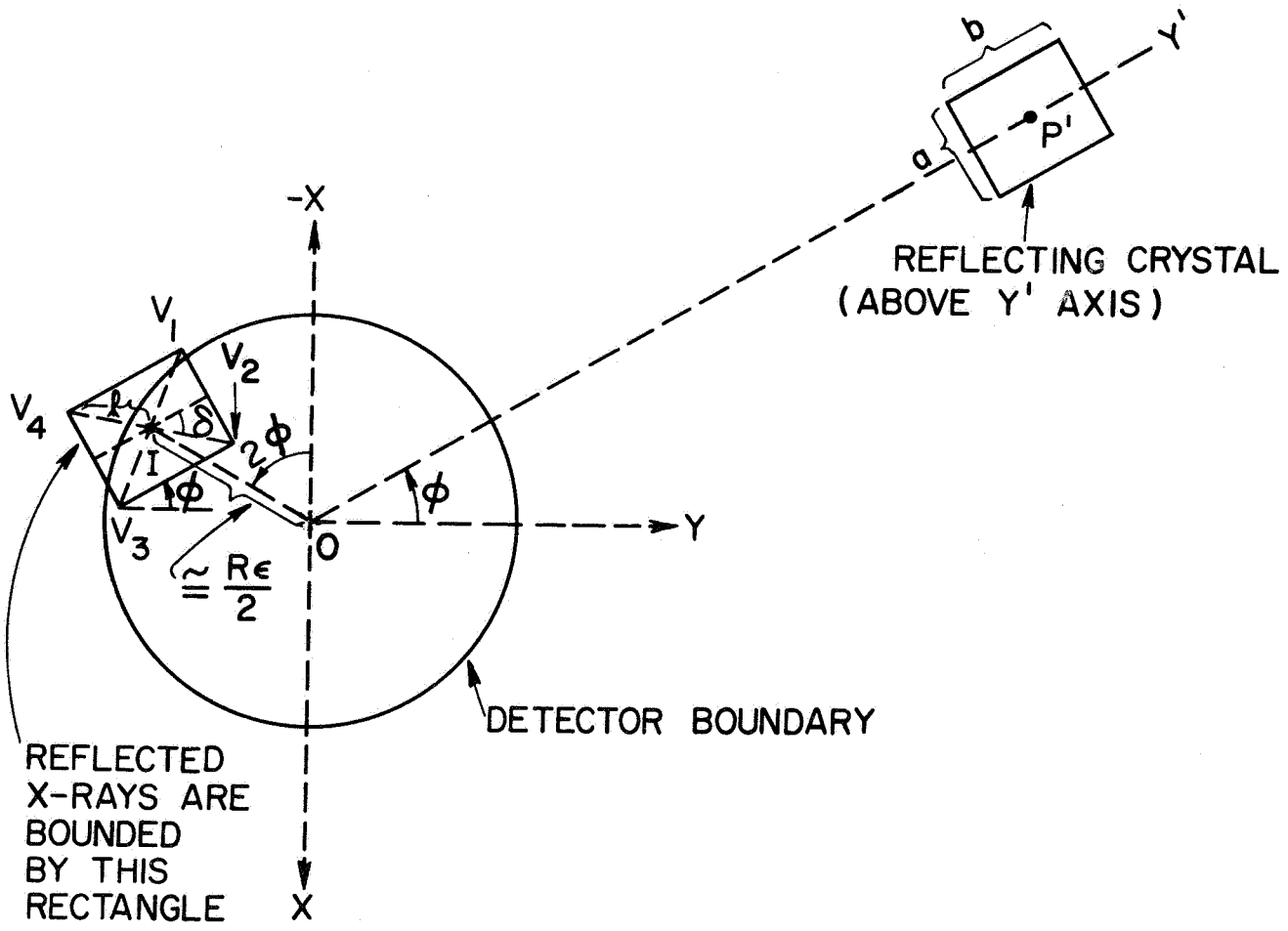

Figure 20. Top view of a reflecting crystal and the boundary of the reflected beam in the detector's plane. The x-ray source is far above the positive x-axis, at a small angle ϵ from the z-axis (which points out of the page).

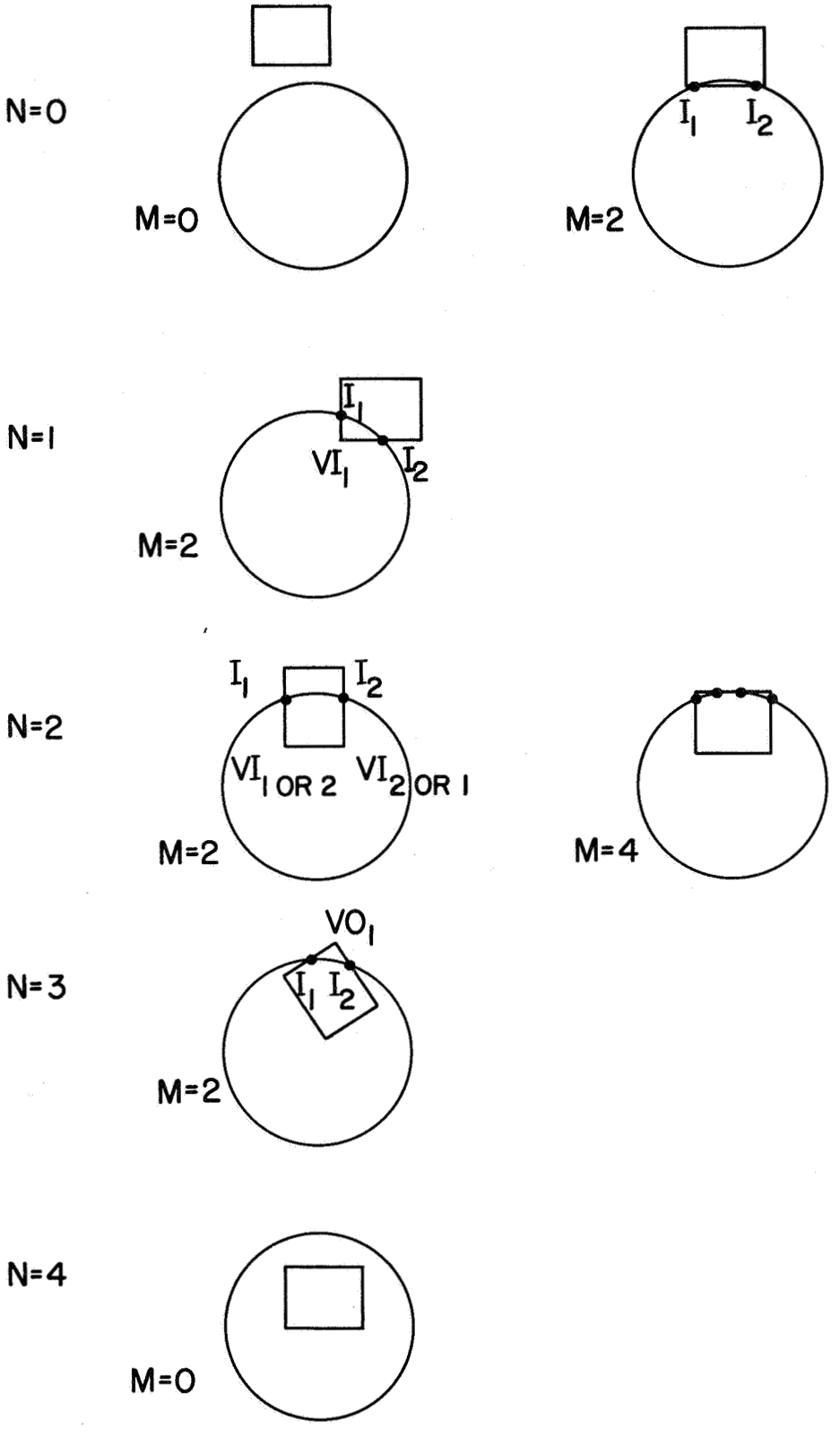

Figure 21. Possible intersection of a rectangle with a circle.

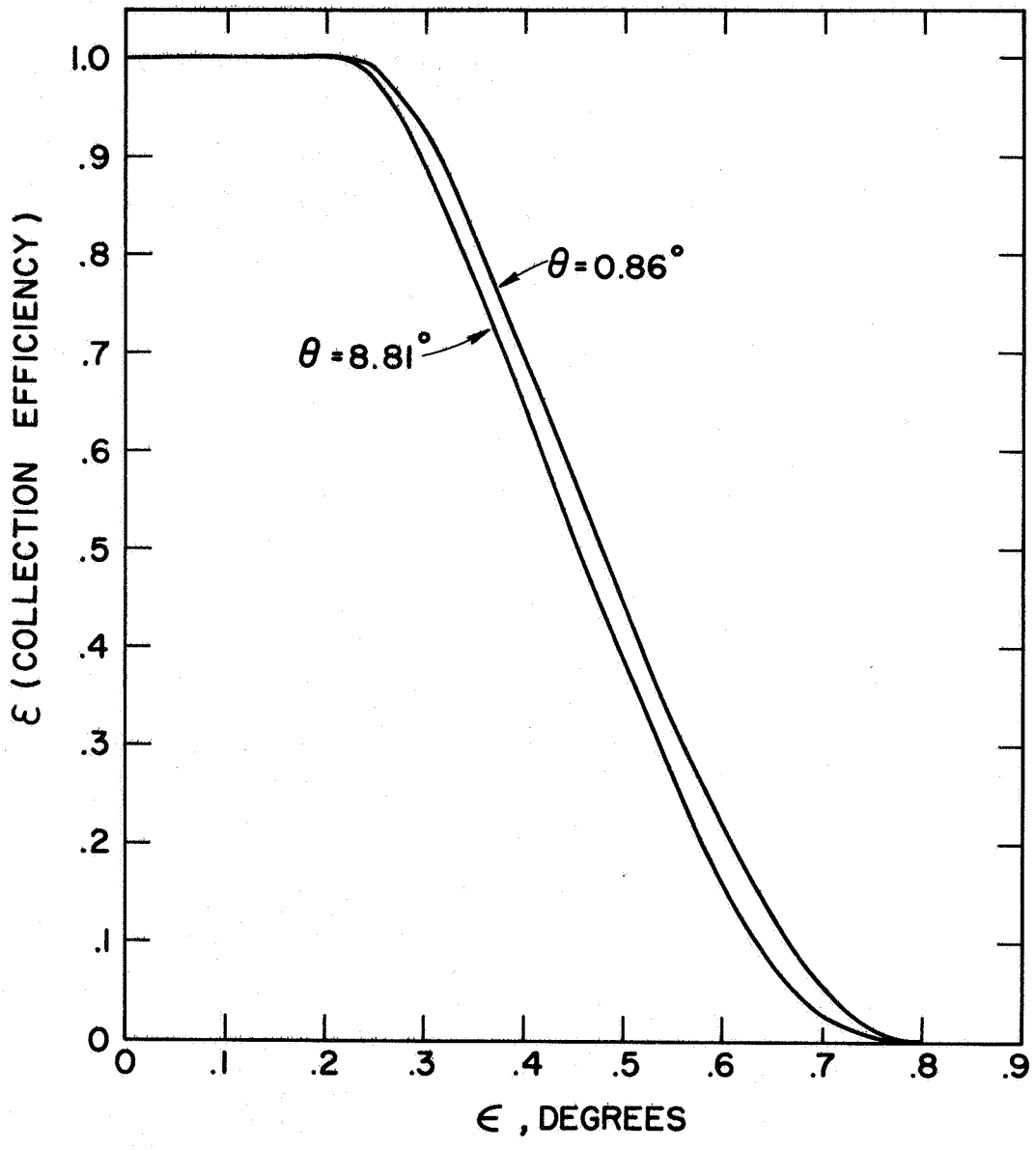

Figure 22. Collection efficiency as a function of the off-axis angle.

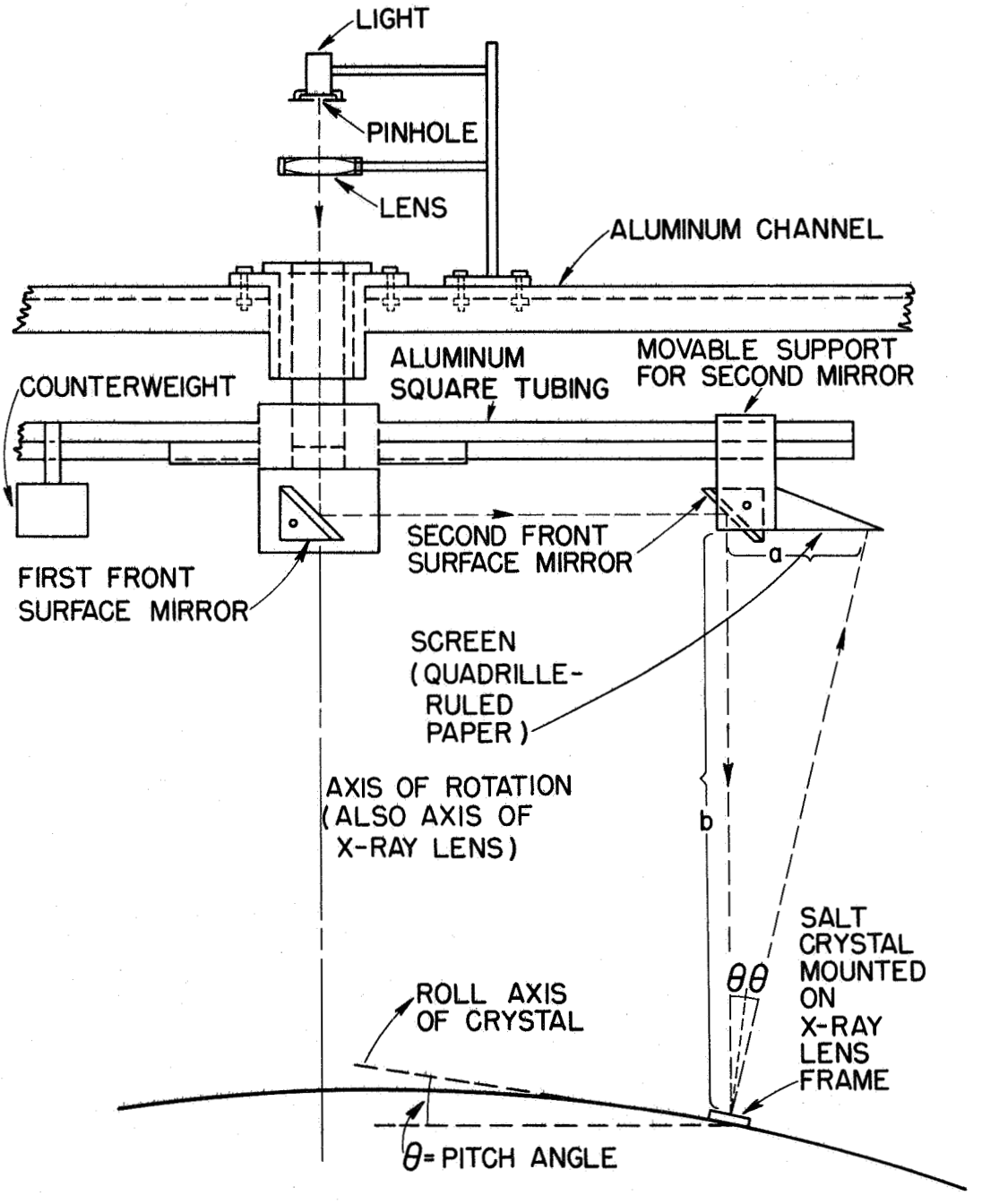

Figure 23. Optical tester for x-ray lens.

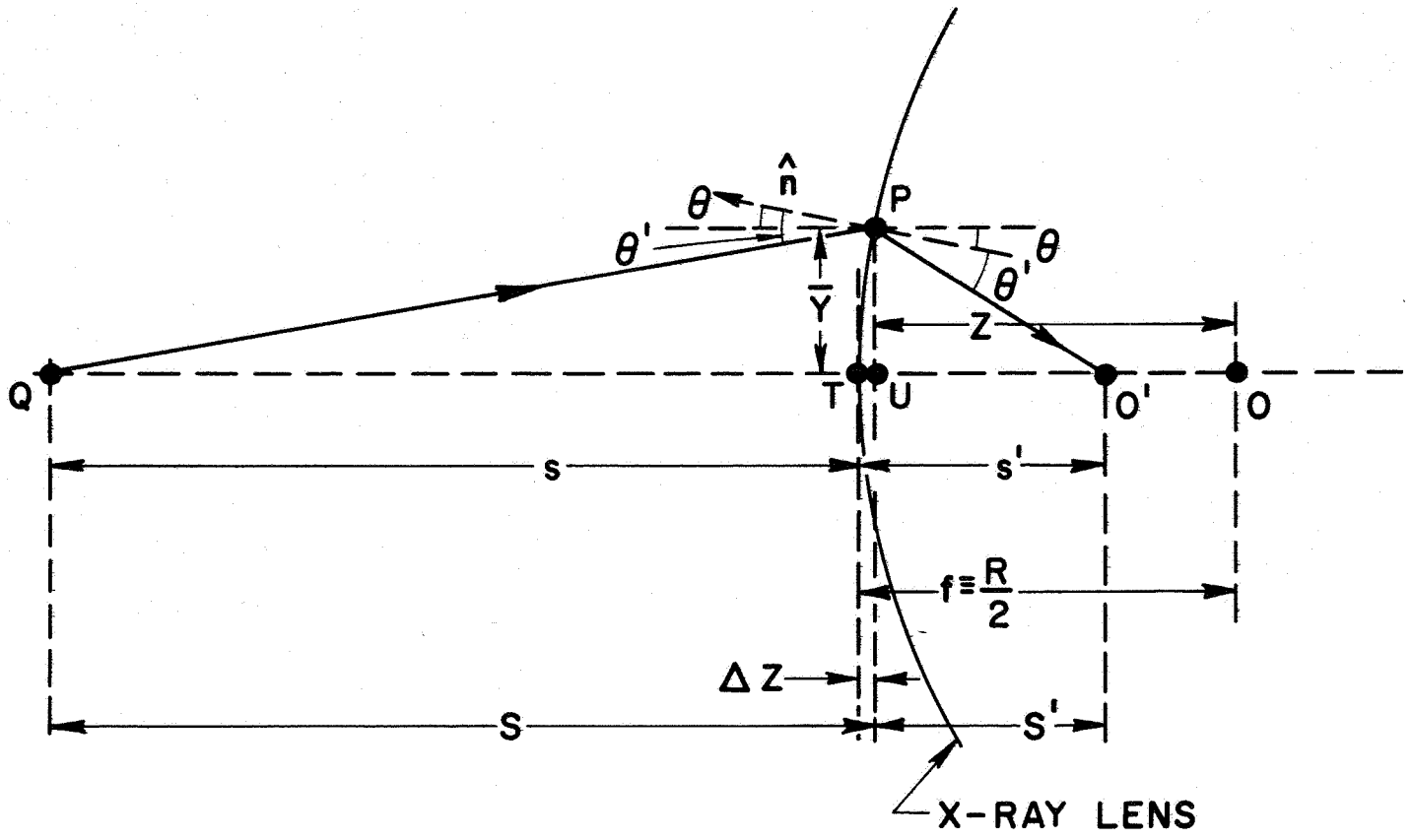

Figure 24. Geometry of focusing x-rays from a source a finite distance away from the lens.

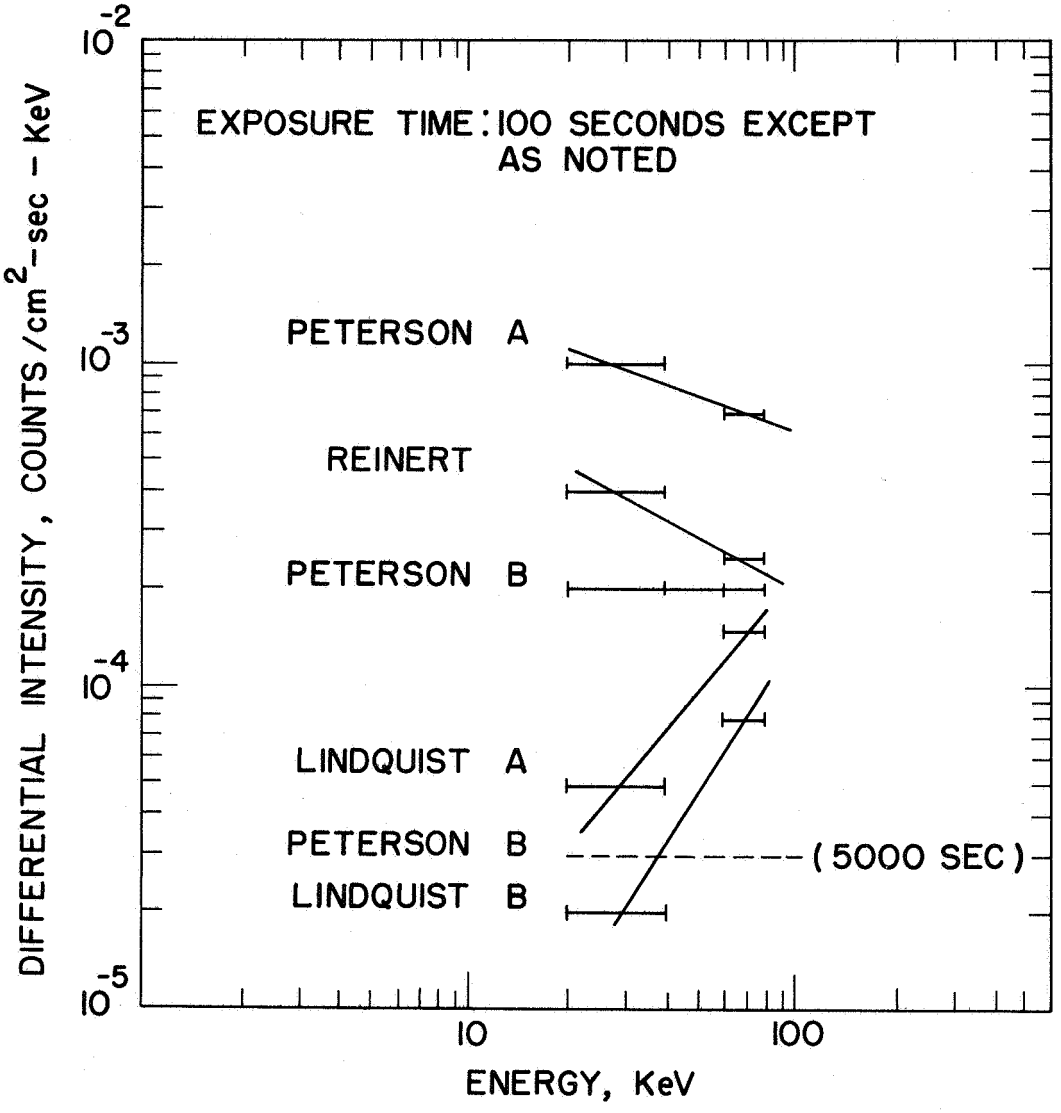

Figure 25. Minimum Source Intensities Required by Various X-ray Detectors.

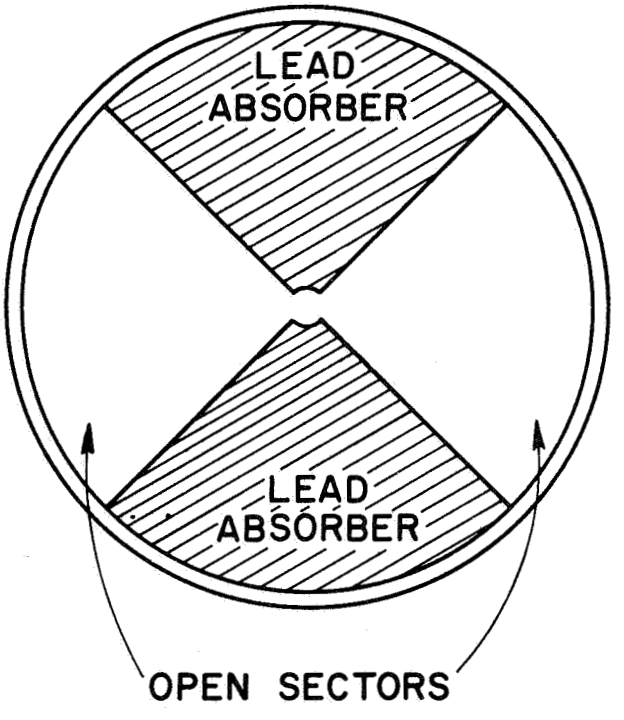

Figure 26. Rotating absorber to be placed under lens to determine polarization.